BNWL-166

AEC RESEARCH and DEVELOPMENT REPORT

QUARTERLY PROGRESS REPORT METALLURGY RESEARCH SECTION JULY, AUGUST, SEPTEMBER, 1965

THE STAFF OF METALLURGY RESEARCH SECTION

OCTOBER 15, 1965

BATTELLE-NORTHWEST
RICHLAND, WASHINGTON

PACIFIC NORTHWEST LABORATORY operated by BATTELLE MEMORIAL INSTITUTE

LEGAL NOTICE

PACIFIC NORTHWEST LABORATORY
RICHLAND, WASHINGTON
operated by
BATTELLE MEMORIAL INSTITUTE
for the
UNITED STATES ATOMIC ENERGY COMMISSION UNDER CONTRACT AT(45-1)-1830

PRINTED BY/FOR THE U. S. ATOMIC ENERGY COMMISSION

AEC-RLOO RICHLAND, WASH.

BNWL-166
UC-25, Metals,
Ceramics, and Materials

FIRST UNRESTRICTED TID-4500

DISTRIBUTION MADE EDITION

QUARTERLY PROGRESS REPORT METALLURGY RESEARCH SECTION JULY, AUGUST, SEPTEMBER, 1965

By

Staff of Metallurgy Research Section

J. J. Cadwell	Manager, Metallurgy Research Section
T. K. Bierlein	Manager, Physical Metallurgy Unit
A. L. Bement	Manager, Reactor Metals Research Unit
R. L. Dillon	Manager, Chemical Metallurgy Unit
R. G. Wheeler	Manager, Materials Engineering Unit

October 15, 1965

PACIFIC NORTHWEST LABORATORY
RICHLAND, WASHINGTON

The information contained in this document represents progress made during a quarter. The data are preliminary and the conclusions are subject to change. Data or conclusions may not be extracted from this document for publication without explicit approval of the author.

Printed in USA. Price $3.00. Available from the
Clearinghouse for Federal Scientific and Technical Information
National Bureau of Standards
U.S. Department of Commerce
Springfield, Virginia

Previous reports in this series:

HW-76228	October, November, December, 1962
HW-77052	January, February, March, 1963
HW-77954	April, May, June, 1963
HW-78962	July, August, September, 1963
HW-79766	October, November, December, 1963
HW-81269	January, February, March, 1964
HW-82651	April, May, June, 1964
HW-84281	July, August, September, 1964
HW-84573	October, November, December, 1964
BNWL-79	January, February, March, 1965
BNWL-120	April, May, June, 1965

TABLE OF CONTENTS

Page

CHEMICAL METALLURGY UNIT

MATERIALS ENGINEERING UNIT

SUMMARY

PHYSICAL METALLURGY UNIT

PLUTONIUM PHYSICAL METALLURGY

The effect of applied uniaxial tensile and compressive stresses on the temperature for the start of the $\beta \rightarrow \alpha$ transformation has been established and explained on the basis of a martensitic type transformation. Evidence that deformed α-plutonium does anneal at 105 °C has been obtained from subsequent $\alpha \rightarrow \beta$ transformation rates; it was established that transformation rates decrease with annealing.

The temperature dependence of the creep of beta plutonium, both beta formed from alpha and beta formed from gamma, was determined at compressive stresses up to 10,000 psi. The creep activation energies for β_γ are 10 to 20% higher than the corresponding values for β_α at 7500 and 10,000 psi.

Deterioration in the rolling behavior of ingots of electrorefined plutonium during a one year storage period in vacuum was attributed to cracking; the effect of helium generation and accumulation on deterioration was therefore masked.

Alpha plutonium rolled in the alpha phase develops a texture which has been studied by X-ray diffraction techniques. Recent results and their interpretation cast considerable doubt on the validity of a [020] texture.

RADIATION EFFECTS ON METALS

Initial investigations by electron microscopy of irradiated high purity nickel show the presence of small defect clusters $\simeq$ 75 to 150 Å in diameter after irradiations of 2.5×10^{18} nvt. Significant annealing of the radiation damage occurs at temperature of 400 °C and above, as shown by the growth of dislocation loops and the reduction in the number of spot defects. Analogies can be made between the irradiation damage and postirradiation annealing behavior in nickel and molybdenum.

An X-ray low-angle scattering apparatus has been installed and experimentation has begun. Significant low-angle scattering was not found in high purity molybdenum until after doses of 1×10^{20} nvt were obtained. Low angle scattering was observed in both unirradiated and irradiated molybdenum containing 100 to 200 ppm carbon. The presence of carbide precipitates may be contributing to the low angle scattering but the effect of double Bragg reflection cannot be ruled out.

DAMAGE MECHANISMS

Analysis of thermally activated deformation in neutron irradiated iron and molybdenum indicates that obstacles which block thermally activated motion of dislocations are submicroscopic. Larger defects, ~50 Å in diameter, revealed by transmission electron microscopy, contribute primarily to the long range athermal stresses. The changes in activation volume during deformation are compatible with dislocation motion confined to localized regions.

SWELLING OF IRRADIATED FISSIONABLE MATERIALS

Factors which influence the degree and type of swelling of fissionable materials during irradiation are being investigated so that mechanisms of swelling can be deduced. Three capsules containing a variety of dilutely alloyed uranium specimens are now under irradiation and will provide information on beta phase operation at 700 °C and on the effect of pressure, 500 psi, on alpha phase operation at 550 and 625 °C. Construction of capsules for irradiating specimens to higher burnups and under different conditions of pressure and temperature has progressed.

The effect of 1000 psi pressure versus 20 psi pressure on swelling of uranium with and without additives at a temperature of 625 °C has been evaluated. The effect of pressure decreases in the order high purity uranium, U + Fe-Si, and U + Fe-Al-Si.

REACTOR METALS RESEARCH UNIT

IN-REACTOR MEASUREMENTS OF MECHANICAL PROPERTIES

The purpose of in-reactor measurements is to determine the effects of fast neutron irradiation on the mechanical properties of structural materials. In-reactor creep measurements are currently being conducted on annealed 304 SS and annealed Zircaloy-2. Creep-rupture studies of Hastelloy X at high temperature are continuing.

In-reactor and out-of-reactor creep rates of 3.3 and 2.5 x 10^{-6}/hr were measured for annealed 304 SS after 2500 hr of testing at 550 °C and 30,000 psi stress. Specimen failure after 2800 hr was observed at a reduced creep-rupture life since the unirradiated creep test is continuing after 4000 hr.

The creep rate measured in-reactor for annealed Zircaloy-2, tested at 315 °C and 15,000 psi, is on the order of 1 to 4 x 10^{-7}/hr. This rate was determined after 1000 hr of testing during which time considerable power fluctuations in the PRTR were encountered. No significant differences in creep rates during reactor outages as compared to reactor operating periods were observed. The creep rate of the out-of-reactor control test was 1.9 x 10^{-7}/hr. It might well be assumed that under the conditions of this test there is little effect of irradiation on the creep of annealed Zircaloy-2.

Creep rupture tests on Hastelloy X are continuing at a temperature of 1950 °F and have been completed at 2100 °F.

The low stress, high temperature decrease in rupture life and minimum creep rate of this alloy in vacuum is similar to the results on nickel-base alloys reported by other investigators. Their work showed that Nichrome V and nickel had better rupture strength in air at low stress while at high stress the reverse was true, i.e., higher rupture strength in vacuum. This can be explained on the basis of two competing processes,

(1) oxidation strengthening and (2) reduction in strength due to a lowering of the surface energy. Air strengthening can be due to one or more processes. Surface oxidation may act as a barrier to dislocations, while internal oxidation reduces the stress concentration by blunting a crack tip. Surface energy effects due to gas adsorption do not play a major role in this investigation since the tests were carried out in vacuum at pressures to 5×10^{-5} Torr.

At low stresses and high temperatures there is a definite decrease in rupture life and minimum creep rates. The decrease in rupture properties has also been noted by other investigators. These investigators assumed that vacuum data represented the intrinsic strength of the alloy; therefore, decrease in vacuum creep rupture properties supports the mechanism of air strenghtening. Hastelloy X is an oxidation resistant alloy; therefore, a very high temperature of transition to air strengthening at reasonable rupture times would be expected.

WELD ZONE FRACTURE TOUGHNESS DETERMINATION

Recent tests were performed to determine the fracture toughness of welded ASTM A302-B steel. Double cantilever beam (DCB) specimens were machined from the mid-thickness of a 1 in. plate containing a double bevel butt weld. The length of the DCB specimen was oriented perpendicular to the weld.

After welding and machining, the specimens were austenitized at 1750 °F for 1/2 hr and water quenched. Fracture toughness determinations were made at room temperature.

These tests indicate that the welded zone is tougher than the base metal, with a peak of maximum toughness in the filler metal, a saddle point immediately adjacent to it, and another toughness maximum in the heat affected zone. The toughness then slowly decreases to a constant value in the base metal. The hardness profile shows correspondence with the maximum toughness region in the filler metal, but there is no hardness drop in the heat affected zone to correspond with the second maximum. This points

out that the fracture toughness is not directly related to the hardness, but is more sensitive to the microstructure of the material.

A second specimen which was stress relieved at 600 °C for 1/2 hr had a similar toughness profile. It was seen that the heat treatment had less effect upon the toughness in the heat affected zone than that of the weld zone. The stress relieved sample had a generally higher fracture toughness.

The nature of the fracture toughness profile obtained indicates that three factors affecting the toughness are: (1) the grain size, (2) the amount of stable carbide precipitation, and (3) the phases present in the microstructure.

These preliminary tests demonstrate the usefulness of the DCB specimen in examining the fracture toughness of a welded material. With a single DCB specimen it is possible to determine the entire toughness profile across the weld. The effect of various heat treatments can readily be observed due to: (1) the sensitivity of the method to changes in the microstructure, and (2) the ease with which the tests may be performed. Further tests are soon to be underway to ascertain the effect of both preweld and postweld heat treatments.

CHEMICAL METALLURGY UNIT

Samples of Haynes Alloy 25, Hastelloy X-280, and Nichrome were prefilmed with oxide of various thicknesses in air at 2050 °F to determine if these films constituted barriers to metal evaporation. Upon exposure to static vacuum conditions at the same temperature, all oxides formed lost adherence and continuity, and allowed the substrate metal to evaporate.

Studies are in progress to determine the dependence of metal evaporation rates in zirconium gettered flowing helium as a function flow rate. Gas purity, temperature, pressure, and general range of gas flows simulate ATR Gas Loop conditions.

The application of small dc potentials to a Zircaloy-2 cathode in process water was found to induce hydrogen absorption by the Zircaloy.

The potential may be applied or generated by a galvanic couple. The efficiency of the hydrogen pickup is higher in the early stages of the hydriding process and at the lower potentials. The effect of ac on this process is not certain.

Prefilmed Zircaloy-2 was vacuum annealed inside and outside a shield made from Zircaloy-2. The postanneal oxidation behavior of shielded and unshielded samples was comparable, indicating no effect of nitrogen or silicon impurities picked up during the anneal. On coupons annealed to completely dissolve the oxide films, the postanneal oxidation rate increased immediately and underwent a marked transition 15 to 25 days after the anneal. Removal of ~3000 Å from the annealed surface by etching in an aqueous HNO_3-HF solution suppressed the first acceleration, but the transition occurred as in the case of unetched coupons.

MATERIALS ENGINEERING UNIT

PRTR PRESSURE TUBES

Properties of Irradiated PRTR Pressure Tubes

Study and testing done during the last quarter year regarding the ability of the PRTR Zircaloy-2 pressure tubes to sustain the PRTR reactor system loads with ever-increasing neutron exposure consisted of: tensile testing of ring specimens after annealing at 550 °F for 2000 hr, a burst test and a crack propagation test of specimens taken from a discharged tube, and measurement of elastic hoop and axial strain on an unirradiated tube specimen during simultaneous application of pressures and axial loads. The tests indicated that 2000 hr at 550 °F did not significantly alter the ring tensile properties as irradiated to 5×10^{20} fast nvt ($E > 1$ MeV), that the burst test and crack propagation failure pressure were equal to or greater than those for specimens having less exposure, and that comparison of the measured strains with calculated strains for a theoretical isotropic body was evidence of anisotropy of the Zircaloy-2 specimen.

GAS LOOP OPERATION

Model Loop Helium Cleanup

Improvements in the gas cleanup system have made it possible to clean up the gas in the model helium loop to less than 1 ppm total impurities at low temperatures The loop was operated at varying flows and temperatures, and measurements were made on the pressure drop in the regenerative heat exchanger. The maximum drop in the shell side of the exchanger was 16.5 in. of water while the pressure drop in the tube side was 9.5 in. of water.

Columbium Sleeve Leak Test

Leakage flow tests on the labyrinth seal for the ATR Gas Loop heat shield were conducted for shield temperatures up to 1000 °F. Problems with the heater have prevented the tests being run up to 2000 °F as required.

Mechanical Tubing Connector Leak Test

A mechanical tubing connector was tested for helium service. The connector was temperature cycled between -190 and 160 °C. One connector was disassembled and reassembled 15 times. No leaks occurred on any of the tests with the helium pressure at 2100 psig.

Model Gas Loop Heater and Piping Modifications

Initial assembly has begun on a model gas loop heater designed to incorporate and investigate essential details of a compact two-stage, concentric heater being designed for the ATR Gas Loop.

Metallic foil insulation sections for the heater and piping are 90% complete.

Molybdenum heating element tubes were successfully joined to their electrical connectors by press-fitting.

Flexible connectors between internal and external electrodes are being rebuilt to use nickel braid instead of nickel sheet.

N-REACTOR

Fracture Studies

A reproducible drop-weight test has been developed to determine the nil ductility transition (NDT) temperature of Zircaloy-2 pressure tubing using specimens cut from the tube wall. The principle of the test is similar to that of the standard drop-weight test for steel. Results show a dependence of the NDT on hydrogen content of the specimen that is consistent with data independently generated in England.

Results of fracture tests on slotted tube specimens covering a wide range of temperatures have been used to construct a fracture analysis diagram. Failure occurs for a given defect size at the same fraction of yield strength for all temperatures from below the NDT to above the crack arrest temperature. This behavior differs from that of steel plate in that the latter exhibits a marked rise in failure stress at temperatures above the NDT.

USA-AECL COOPERATIVE PROGRAM

Zr-Nb Pressure Tubing

Crack propagation of hydrided Zr–2.5 wt% Nb alloy appears to be somewhat erratic as compared to Zircaloy-2. Tensile tests reveal little or no effect of varying strain rate at 23 and 300 °C. A small effect is observed at 400 °C.

PHYSICAL METALLURGY UNIT

PLUTONIUM PHYSICAL METALLURGY - F. E. Bowman, H. E. Kissinger, B. Mastel, and R. D. Nelson

The objective of this program is to conduct basic studies on the properties of high purity unalloyed and alloyed plutonium. Studies include investigation of phase transformation, phase stabilization, deformation, fracture, texturing, internal stresses, microcracking, grain growth, recovery and recrystallization, and measurement of mechanical and physical properties. The unique structure of several of the plutonium allotropes and their narrow temperature span of stability leads to characteristics and anomalies which, if explained, will contribute to the general area of solid state science.

Effect of Applied Stresses on the $\beta \rightarrow \alpha$ Transformation

The effect of applied uniaxial tensile and compressive stresses on the $\beta \rightarrow \alpha$ transformation was investigated to provide indirect information on the nature of this transformation. More specifically, the $\beta \rightarrow \alpha$ starting temperature was determined as a function of stress at a cooling rate of 2 °C/hr. The results are characteristic of a martensitic transformation.

Applied compressive stresses up to 10,000 psi raised the $\beta \rightarrow \alpha$ starting temperature of electrorefined plutonium 1.2 °C/1000 psi and applied tensile stresses raised the starting temperature 0.4 °C/1000 psi, Figure 3.1. The data clearly show that applied uniaxial compressive stresses favor the plutonium $\beta \rightarrow \alpha$ transformation more than applied uniaxial tensile stresses. This is to be expected because of the 9% volume decrease accompanying the $\beta \rightarrow \alpha$ transformation. However, the starting temperature is increased more by applied stresses than can be explained on the basis of only volume change. Actually, on the basis of only volume change tensile stresses should oppose the $\beta \rightarrow \alpha$ transformation and consequently lower the starting temperature.

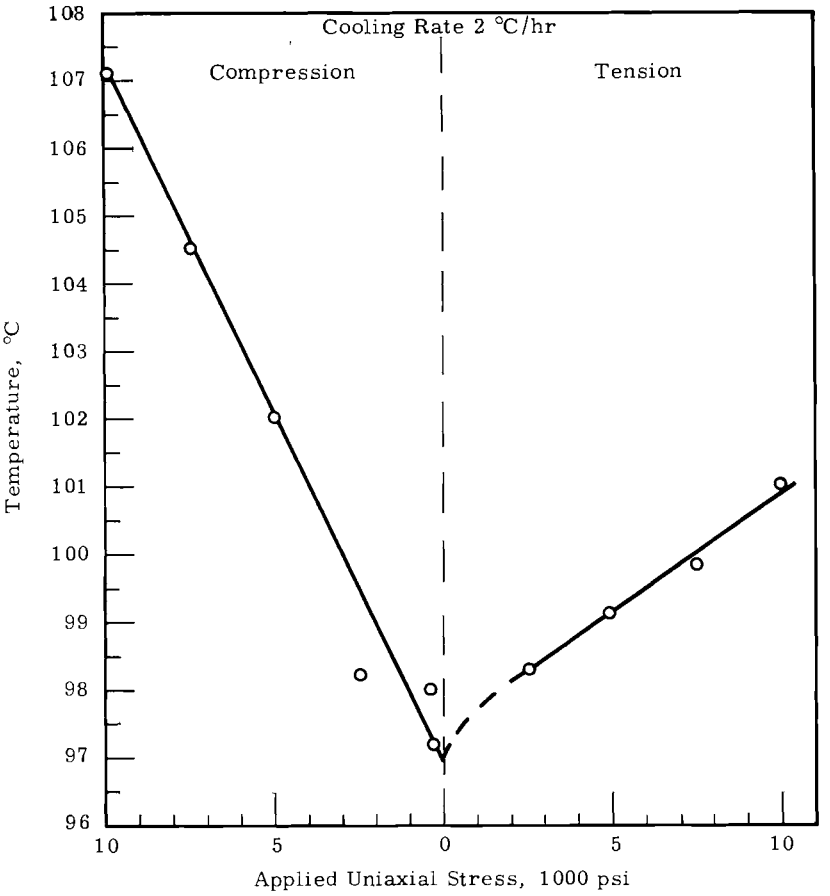

FIGURE 3.1

Effect of Applied Uniaxial Stress on the Temperature for the Start of the $\beta \rightarrow \alpha$ Transformation in Plutonium

The behavior of plutonium during the $\beta \rightarrow \alpha$ transformation under applied stresses is completely in keeping with the hypothesis that the $\beta \rightarrow \alpha$ transformation is martensitic. Similar effects were reported for the plutonium $\alpha \rightarrow \beta$ transformation and were compared to martensitic transformations in other materials.

All shear stresses favor martensitic transformations, regardless of the volume change, but normal components of applied stresses favor or oppose martensitic transformations depending on whether contraction or expansion accompanies the transformation. The shear stresses of both types of applied stresses and the normal component of compressive

stresses favor the plutonium $\beta \rightarrow \alpha$ transformation but the normal component of tensile stresses should oppose the plutonium $\beta \rightarrow \alpha$ transformation if it is a martensitic transformation. Thus, the data on the plutonium $\beta \rightarrow \alpha$ transformation are consistent with the behavior of known martensitic transformations.

Temperature Dependence of the Specific Volume of Alpha-Plutonium

The specific volume of α-Pu was measured as a function of temperature between 95 and 115 °C to see if a discontinuity exists in specific volume at high alpha temperatures before the $\alpha \rightarrow \beta$ transformation begins. Four specimens were heated at a rate of 2 to 3 °C/hr. No discontinuity, within an experimental error of $\pm 2.5 \times 10^{-5}$ cm^3/g were observed in specimens that had been either (1) as-cast, (2) annealed 66 hr at 105 to 110 °C, (3) quenched from the beta phase to -75 °C, or (4) β to α isothermally transformed at 85 °C. A specimen adjacent to these four was sent to Mound Laboratory. At that site Selle found a discontinuity in the specimen at 105 °C in the differential thermal analysis trace.[1] If the process responsible for the observed discontinuity at 105 °C is also responsible for a volume change, then the volume change must be less than the limit of sensitivity of volume change measurements.

Annealing of Deformed Alpha-Plutonium

Deformed α-Pu specimens were annealed at 105 °C to determine whether cold work could be annealed out of α-Pu. The $\alpha \rightarrow \beta$ transformation rate was used as a measure of the annealing since deformation accelerates the $\alpha \rightarrow \beta$ transformation rate. The basis of the tests was that the $\alpha \rightarrow \beta$ transformation rate would decrease as the specimens were annealed. Accordingly, seven specimens were compressed to one half their thickness at 60 °C. They were then annealed for different times at 105 °C. The results showed that deformed α-Pu can be annealed at 105 °C. They also showed 2 wk were necessary to complete the annealing process as measured by the $\alpha \rightarrow \beta$ transformation rate, Table 3.1. These results are to be supplemented with resistivity measurements.

---

1. J. E. Selle. Unpublished Data, Monsanto Corporation, Mound Laboratory, Miamisburg, Ohio. June, 1965. (Personal Communication)

TABLE 3.1

ANNEALING OF DEFORMED ALPHA-PLUTONIUM AS REVEALED BY THE INCUBATION TIME* AND THE TIME FOR 50% TRANSFORMATION OF THE $\alpha \rightarrow \beta$ TRANSFORMATION

Annealing Time at 105 °C hr	Times required for $\alpha \rightarrow \beta$ Transformation at 119 °C	
	Incubation Time	Time for 50% Transformation
0	350	2,240
1	1300	4,000
2	2000	7,200
4	3000	9,500
24	3500	9,800
120	5300	12,000
700	5500	12,300

* Incubation time is defined as the time for the first detectable amount of transformation.

Creep of Beta Plutonium

Experiments on the creep of β-Pu were performed to elucidate observations that are not consistent with creep of most metals. Five such observations are: (1) the creep rates of β-Pu formed from α-Pu, β_α, are 50 to 300 times the creep rates of β-Pu formed from γ-Pu, β_γ, (2) the creep rates of β-Pu do not appear to depend on the modulus of elasticity, (3) the creep activation energy of β-Pu is very dependent on the applied stress, (4) the dependence on stress of the β_α creep rate is not the same as reported for most metals, and (5) the creep of β_α is not always linear.

Thus, the creep rates of β-Pu were determined as a function of temperature and as a function of stress so that deformation of β-Pu by creep may be better understood. Also, these experiments are providing further information that will aid in explaining the differences between β_α and β_γ. The creep activation energy was computed from the data at different stresses.

A compression creep apparatus was used to perform the experiments. The platens and the specimen were immersed in a high temperature silicone fluid so that the temperature could be controlled within ±0.5 °C and so that

the specimen would come to thermal equilibrium more rapidly than if the specimen were in a vacuum. The specimens were 0.20 in. diam rods made from electrorefined plutonium.

The temperature dependence of the creep of β_α was determined at 1500, 2100, 2900, 4000, 5500, 7600, and 10,000 psi. For creep of β_α, the plots of log $\dot{\epsilon}$ as a function of 1/T were linear at the low beta temperatures, but they were nonlinear at the higher temperatures, Figure 3.2. The higher the stresses, the lower the temperatures where the curves deviated from linearity. For example, the deviation occurred at 135 °C with a stress of 10,000 psi and it occurred at 185 °C with a stress of 2100 psi. No deviation occurred with a stress of 1500 psi.

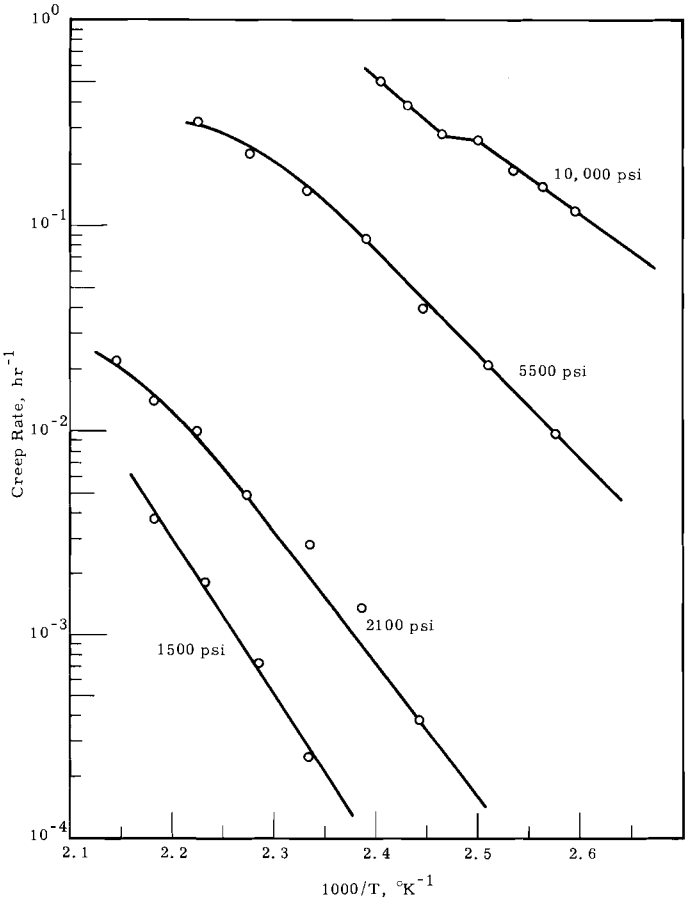

FIGURE 3.2

Temperature Dependence of the Creep of β-Pu Formed from α-Pu

Similar plots for creep of β_γ were linear at all temperatures, Figure 3.3. Linearity of these curves shows that the large temperature change in modulus of elasticity, $dE/dT = -8 \times 10^3$ psi/°C, for the beta phase does not influence the creep rates. If the creep rate is related to modulus of elasticity as proposed by Sherby[1] then the log strain rate versus 1/T plots would not be linear but would instead have a slope that increases with decreasing values of 1/T.

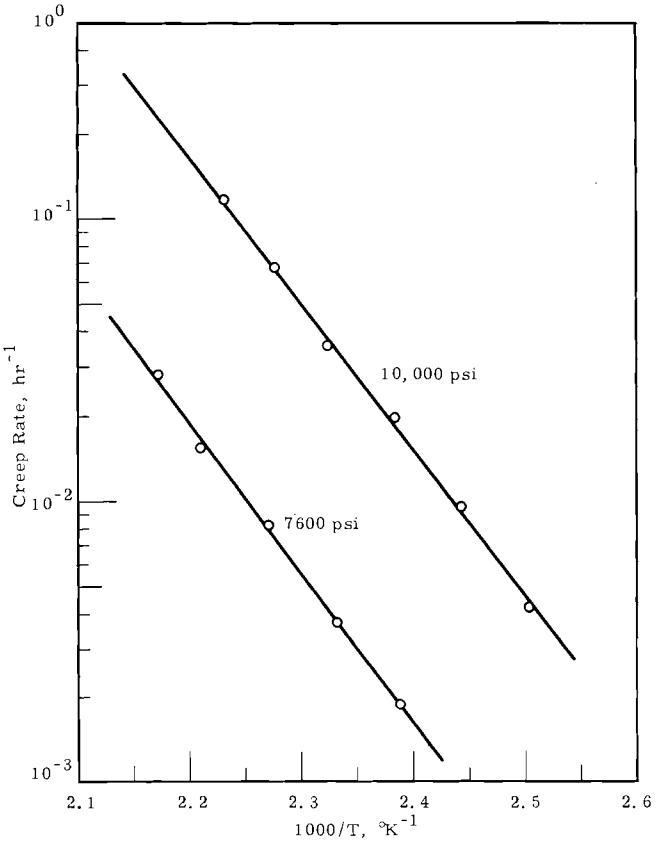

FIGURE 3.3

Temperature Dependence of the Creep of β-Pu Formed from γ-Pu

The creep activation energy was calculated from the linear portion of each curve by applying the Arrhenius relationship, $\dot{\varepsilon} = Ae^{-Q/RT}$. The β_α creep activation energy depended upon stress as shown in Figure 3.4. The creep activation energy for β_γ was 10 to 20% higher than it was for β_α at 7500 and 10,000 psi.

1. O. D. Sherby. Acta Met., vol. 11, p. 591. 1963.

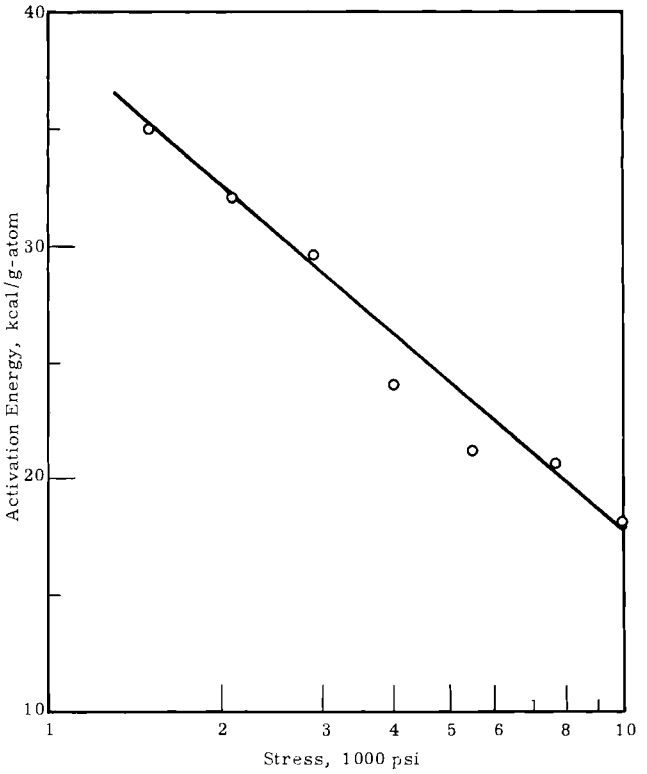

FIGURE 3.4

Effect of Applied Compressive Stresses
on the Activation Energy of Beta Plutonium
(The beta phase was formed from the alpha phase.)

The steady-state creep rate is related to the stress by the proportionality $\dot{\epsilon} \alpha \sigma^n$ for most metals. For β_γ, n is a constant and equals 5. This is the value for most metals at strain rates between 10^{-4}/hr and 10^{-1}/hr. For β_α, n = 5 at strain rates of about 10^{-4}/hr, but it is < 5 at higher and lower strain rates.

The investigations in progress will supply data needed to explain the deviation from linearity of the log $\dot{\epsilon}$ versus 1/T curves for β_α. In addition, the β_α creep rates will be measured at stresses of 500, 1000, and 14,000 psi and the β_γ creep rates will be measured at 2100, 2900, 4000, 5500, and 14,000 psi. These data should provide a good comparison of β_α creep and β_γ creep.

Deformation and Fracture Mechanisms

Evidence has previously been presented which suggests that the self-damaging processes resulting from the radioactive decay in plutonium effect a significant deterioration in the rolling behavior of the metal. A further indication of this deterioration has recently been obtained during attempts at rolling castings which had been aged over 1 yr. These samples were portions of ingots of high purity electrorefined plutonium. As freshly cast, portions of the original ingots had been successfully rolled without difficulty.

The aged pieces, which had been stored in vacuum to minimize hydrogen contamination, were found on metallographic examination to contain a large number of microcracks. These had not been evident in the freshly cast material. As might be expected, this cracked material failed to survive the first pass through the rolls. Unfortunately, these most recent experiments do not conclusively confirm the original hypothesis of self-damage responsibility. Transformation during aging of retained beta could have contributed to the cracking, although the as-cast densities of the ingots were such as to indicate that the amount of retained phase was minimal. In order to establish without question the role of self-damage in metal property deterioration, it will be necessary to conduct experiments on a series of samples with varying and known amounts of Pu^{240} and Pu^{241} in order to predetermine the amount and type of damage to be expected.

Analysis of the details of the rolling texture established in α-Pu, as well as the fiber texture introduced by the transformation from β to α under the influence of uniaxial compressive stress, has been pursued. Several anomalies have been found in the diffraction patterns which suggest that the original conclusion, drawn not only here but at various other sites, that the [010] direction lies in the direction of rolling or in the direction of applied stress in the fiber textured material, may not be valid. The fact that the (020) and (211) reflections are nearly superimposed and are the two strongest lines in the pattern of α-Pu tends to confuse the issue. The characteristics of the (211) reflection can be cited as an example of the anomaly which leads one to suspect a different texture than that previously proposed.

The pattern of the rolling surface of a rolled sample was originally interpreted as indicating the predominance of the (211) plane in this surface. However, the pattern obtained from the longitudinal surface of the sheet, perpendicular to the rolling plane and parallel to the rolling direction, also revealed a strong (211) reflection. Since the (211) plane forms an angle of 60° with the (020), it is difficult to visualize a texture in which the (211) plane could yield intense reflections from two mutually perpendicular surfaces, both of which are in turn perpendicular to a plane containing the (020). The behavior of several other planes is also difficult to interpret on the basis of an (020) texture. An interpretation which will be in accord with the less evident, but perhaps more basic, diffraction effects, is actively being sought.

A correct interpretation and thorough understanding of the textures which can be introduced in α-Pu are essential to an understanding of the deformation processes as well as to the correct interpretation of the interphase crystallographic relationships.

It is interesting to note, as an indication of the present state of the knowledge of α-Pu deformation mechanisms, that B. Spreit (Fontenay aux Roses in France) wrote, "The absence of all other systems of secondary slip removes all ambiguity from the interpretation of the preceding facts and permits the reasonable conclusion that in α-Pu the (020) plane is the major slip plane at ambient temperature."[1] However, Bronisz and Tate of Los Alamos conclude with the statement, "This suggests that the (020) is not the major slip plane in plutonium."[2] The quoted authors derived their data from fiber textured samples. The diametrically opposed conclusions are indicative of the care required in the analysis and interpretation of the diffraction data from the complex monoclinic cell of α-Pu.

---

1. B. Spreit. J. Nucl. Mater., vol. 15, 2nd Issue. 1965.
2. S. Bronisz and R. E. Tate. Trans. Met. Soc AIME. July, 1965.

RADIATION EFFECTS ON METALS - J. L. Brimhall, H. E. Kissinger, B. Mastel, and F. A. Smidt

This program is directed toward establishing the combined effect of impurities and neutron irradiation on the properties and structure of specific metals, and deducing from thermally-activated recovery processes how the damage state can be altered. Present studies involve single and polycrystalline specimens of molybdenum, nickel, and rhenium.

Transmission Electron Microscopy

Radiation damage in nickel, a fcc metal, and rhenium, a cph metal, are being studied in a manner analogous to that of molybdenum, a bcc metal. To date, nickel of four purities (99.997, 99.7, 99.6, and 99.4%) has been irradiated at 60 °C to an exposure of 2.5×10^{18} nvt (E > 1 MeV). Samples comprising two metallurgical states, vacuum annealed and cold-rolled 30%, were irradiated. Foils of the two higher purities in both metallurgical states have also been irradiated to 5 and 10×10^{18}. Induced radioactivity has decayed to a level permitting electron microscope and X-ray studies to begin on the specimens exposed to 2.5×10^{18} nvt.

Transmission electron microscopy of the 99.997% pure nickel has revealed defect clusters which are tilt sensitive. The defect clusters, shown in Figure 3.5a, have a diameter range of 75 to 150 Å. The density of the clusters is approximately $2.5 \times 10^{16}/cm^3$. Resolvable dislocation loops were rarely observed. Denuding adjacent to grain boundaries was not observed in any of the samples. The irradiated foils were annealed in vacuum at 400 °C for 6 hr to induce loop growth. After annealing, the spot density was decreased by an order of magnitude and resolvable loops were present, as shown in Figure 3.5b. The density of the loops was approximately $1 \times 10^{15}/cm^3$ and the loops had a diameter range of 200 to 250 Å. The growth of loops as well as the disappearance of the spots can be explained by clusters acquiring point defects of their own kind. The annealing behavior in nickel is analogous to molybdenum containing 100 to 200 ppm carbon in which the larger loops grow at the expense of the smaller ones.

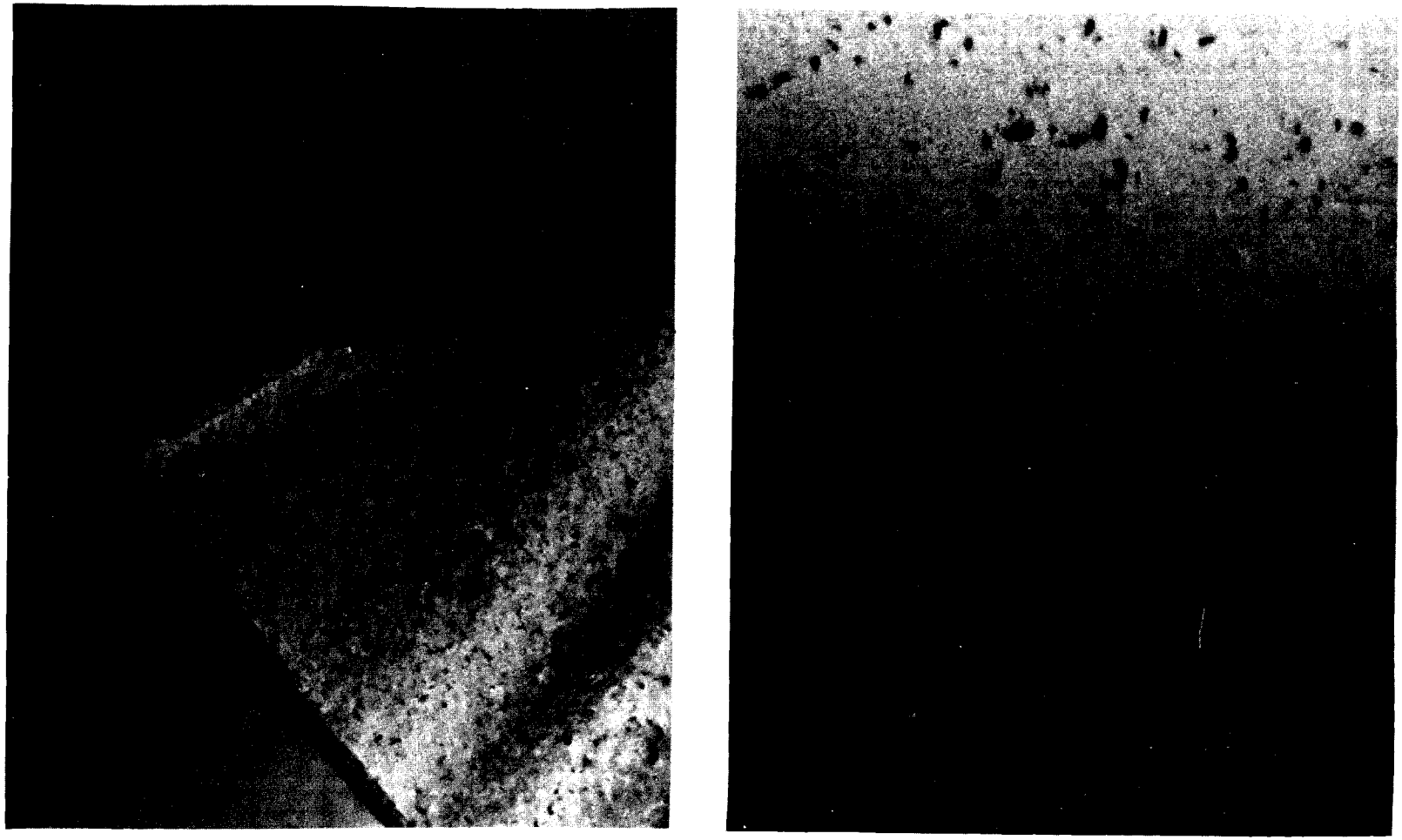

Neg. 3415A; 3441B

(a) As-Irradiated

(b) After Annealing the Irradiated Specimen at 400 °C for 6 hr

FIGURE 3.5

Defect Clusters in 99.99% Pure Nickel
After Irradiation to 2.5×10^{18} nvt at 60 °C

156,000X

Dark field techniques are being used to identify the character of the loops in nickel. A magnetic coil has been installed in the Philips EM 200 electron microscope. The coil permits inclination of the electron beam, making dark field microscopy possible. Dark field micrographs have revealed the presence of interstitial clusters in the irradiated and annealed foils. Specimens are currently being annealed at higher temperatures to induce further loop growth so that crystallographic analysis may be made in conjunction with dark field techniques.

Previous Quarterly Progress Reports have described the role of preexisting dislocations on the density and distribution of defect clusters produced by neutron irradiation in molybdenum. Molybdenum foils were prestrained controlled amounts, irradiated at 60 °C, and studied by transmission electron microscopy. The results show that (1) old dislocations do not act as sinks for interstitial atoms, and (2) vacancies produced during the prestrain alter the final microstructure. Deformation behavior of the prestrained and irradiated samples were more compatible with a source hardening model than with a lattice hardening model. These findings have been described in a paper submitted for publication in Acta Metallurgica.

X-Ray Diffraction Studies

The studies on the effects of neutron irradiation on molybdenum have indicated that the defects observed by electron microscopy are due to clusters of interstitial atoms. No defects positively attributed to the presence of vacancies have been observed in the electron microscope, although length change measurements, stored energy release, and resistivity changes at 150 to 200 °C strongly suggest the presence of vacancies.

A small angle X-ray scattering camera has been installed to investigate the possible presence of vacancies in submicroscopic size clusters. The small-angle technique makes use of the diffraction effects which occur when X-rays are transmitted through a medium of inhomogeneous electron density. If a well collimated, nearly parallel beam of X-rays is used, the small-angle scattering results in a broadening of the beam by a perceptible amount, as much as a few degrees in some cases.

Small-angle scattering data are interpreted in terms of the size of the scattering regions. It has been shown by Guinier[1] that the scattered intensity I(h) is given by

$$I(h) = K \exp\left(-\frac{h^2 R_o^2}{3}\right)$$

where R_o is a quantity called the "radius of gyration," an electron-density analog to the mechanical radius of gyration. It is defined as

$$R_o = \frac{\sum_k \rho_k r_k^2}{\sum_k \rho_k}$$

where ρ_k is the electron density at a distance r_k from the center of the particle. The quantity h is a measure of angle, given by

$$h = 4\pi \frac{\sin \theta}{\lambda} \quad .$$

Experiments have been performed on molybdenum foils of various purities, in the unirradiated condition and after neutron irradiation. Some results are shown in Figure 3.6.

It may be seen that no small-angle scattering appears for high purity molybdenum (<10 ppm C) irradiated to 1×10^{19} nvt (E > 1 MeV), but there is appreciable scattering for exposures of 1×10^{20} nvt. This broadening, when analyzed in terms of radius of gyration, yields an R_o value of about 30 A. The molybdenum containing 100 to 200 ppm carbon shows considerable small-angle scattering in both the unirradiated and irradiated condition. This is probably a result of the precipitation of small carbide particles, although the possibility of a crystallographic diffraction effect (the so-called "double-Bragg scattering") can not be ignored.

Further work will involve the preparation of thinner samples and the use of monochromatic radiation. This will result in better data and will tend to eliminate the possibility of double-Bragg scattering.

---

1. Andre Guinier. Small Angle Scattering of X-rays, John Wiley & Sons, New York, 1955. p. 126-127.

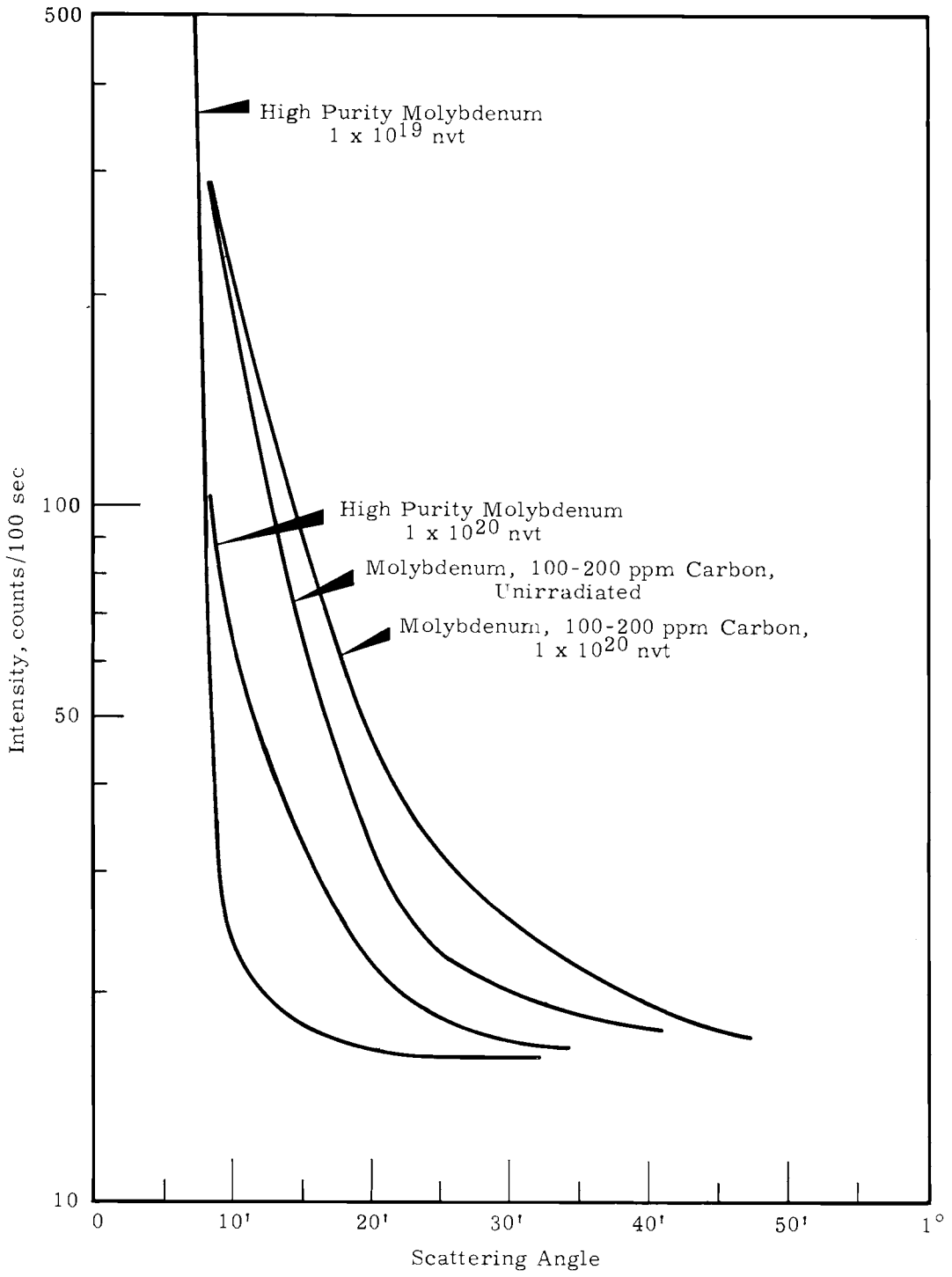

FIGURE 3.6

Small-Angle Scattering
from High-Purity and Carbon-Doped Molybdenum

DAMAGE MECHANISMS - F. A. Smidt and J. J. Laidler

The objective of this program is to determine how the mechanical properties of irradiated iron are modified by interaction of moving dislocations with irradiation induced defects. The method being utilized is the application of thermally activated flow theory to the deformation process in irradiated iron. During this period the following paper was prepared for presentation at the AIME Symposium on Radiation Effects, (Asheville, North Carolina, September 8-16, 1965).

Correlation Between Mechanical Properties and Microstructure in Irradiated Iron and Molybdenum

Introduction

In recent years, transmission electron microscopy and the study of thermally-activated deformation have had considerable impact in the area of dislocation theory. The utility of electron microscopy in the study of irradiation effects in solids has been amply demonstrated by numerous investigators. Little use has been made, however, of thermally-activated flow measurements in such studies, although the capabilities inherent in the technique indicate it should be useful in studying interactions between dislocations and atomic size defects. This report describes the preliminary results of studies on irradiation effects in iron and molybdenum in which both techniques have been used to correlate dislocation dynamics with the direct observation of the defect structure.

Experimental

Polycrystalline specimens of vacuum-melted electrolytic iron (Ferrovac-E), zone-refined iron (Battelle), and high purity sintered molybdenum were irradiated at approximately 60 °C in a Hanford reactor. The composition of these materials is given in Table 3.2. The exposure employed for iron was 5×10^{18} neutrons/cm^2 and for molybdenum 1×10^{18} neutrons/cm^2 ($E > 1$ MeV).

Tensile tests were conducted with an Instron testing machine, at a base strain rate of 3.3×10^{-5} sec^{-1}. Activation volume determinations were carried out as described in a recent review paper.[1]

1. H. Conrad. J. Metals, vol. 16, p. 582. 1964.

TABLE 3.2

COMPOSITIONS OF MATERIALS STUDIED

(Impurity concentrations in ppm)

Impurity	Molybdenum	Ferrovac-E	Zone Refined Iron
Carbon	10	40	3.3
Nitrogen	8	1	<1
Hydrogen	2	--	--
Oxygen	11	200	2.6
Silicon	10	200	10
Nickel	5	20	10
Aluminum	--	--	15
Tungsten	80	--	--

Direct observation of the irradiated microstructure in iron was accomplished by wafering of bulk tensile specimens and electrolytic thinning of the wafers.[1] In the case of molybdenum, 0.003 in. thick foils were irradiated and subsequently electrolytically thinned. The specimens were examined in transmission with a Philips EM-200 electron microscope operating at 100 kV.

Microstructure

The results obtained with transmission electron microscopy on irradiated molybdenum have been reported previously.[2] At an exposure of 1×10^{18} neutrons/cm^2, defects in the form of small spots were observed. The density of these spot defects was about 4×10^{14} cm^{-3}, with an average diameter of 20 to 25 Å. From results at higher exposures and from post-irradiation annealing, it was concluded that the majority of these spot defects are clusters of interstitial atoms. However, as noted in a separate study,[3] the concentration of observable defects is much lower than that deduced by a conservative theoretical estimate, so that most of the point defects produced in molybdenum by neutron irradiation at 60 °C are present as single entities, small complexes, or unresolvable clusters. Annealing of the irradiated molybdenum containing greater amounts of carbon caused resolvable

1. B. Mastel and H. E. Kissinger. J. Sci. Inst., vol. 41, p. 510. 1964.
2. B. Mastel and J. L. Brimhall. Acta Met., to be published.
3. M. E. Downey and B. L. Eyre. Phil. Mag., vol. 11, p. 53. 1965.

prismatic loops to form at the expense of the small clusters of interstitial atoms.[1]

In the case of iron, no spots were observed in the irradiated specimens examined in this study, nor were any observable defects produced by annealing. Other investigators,[2-3] however, have reported spots in iron irradiated to higher exposures, 2×10^{20} neutrons/cm^2. After post-irradiation annealing at temperatures sufficient to cause growth of spots resolvable prismatic loops were observed and were determined to be interstitial in origin, as with molybdenum containing carbon.

Irradiated molybdenum foils[4] and molybdenum single crystals[5] have been deformed and examined in transmission. At an exposure of 1×10^{19} neutrons/cm^2, distinct "channels" free of spot defects are observed as shown in Figure 3.7. These channels were attributed to the motion of dislocations in restricted paths, and have been correlated with gross surface slip traces.[5] Similar observations have been reported on iron[2, 6] as well as nickel[7] and copper.[8]

Thermally-Activated Flow

Activation volume measurements provide an indication of the interaction between atomic size defects and dislocations. The activation volume

---

1. B. Mastel and J. L. Brimhall. Acta Met., to be published.
2. B. L. Eyre and A. F. Bartlett. An Electron Microscope Study of Neutron Irradiation Damage in Alpha Iron, AERE R-4752, Atomic Energy Research Establishment, Harwell, Berkshire, England. November, 1964.
3. J. S. Bryner. A Study of Neutron Irradiation Damage in Iron by Electron Transmission Microscopy, BNL-8832, Brookhaven National Laboratory, Upton, New York. 1965.
4. B. Mastel H. E. Kissinger, J. J. Laidler, and T. K. Bierlein. J. Appl. Phys., vol. 34, p. 3637. 1963.
5. J. L. Brimhall. The Effect of Neutron Irradiation on Slip Lines in Molybdenum, BNWL-44. March, 1965.
6. B. L. Eyre. Phil. Mag., vol. 8, p. 1609. 1962.
7. I. G. Greenfield and H. G. F. Wilsdorf. Naturwissenschaften, vol. 47, p. 395. 1960.
8. A. Seeger. The Relation Between Structure and Mechanical Properties of Metals, H. M. Stationery Office, London, 1965.

FIGURE 3.7

Channels Observed in a Molybdenum Specimen Irradiated to 1 x 10^{19} nvt (E > 1 MeV), Deformed 2% in Tension, Sectioned and Thinned for Transmission Electron Microscopy 75,000X

is determined by the mechanism of dislocation motion and is related physically to the product of the Burgers vector, the length of active dislocation segment and the width of the barrier. The mechanism of thermally activated dislocation movement in bcc metals at low temperatures, 0 °K to about 0.15 T_m, is generally accepted as the Peierls mechanism as described by Dorn and Rajnak.[1] At temperatures above this range the issue is still somewhat in doubt with several possibilities suggested, among them small precipitate particles. It is obvious, however, that if defects introduced by neutron bombardment are to influence the mechanism then a change in activation volume must be observed. Such changes have been observed in both iron[2] and molybdenum.

Iron. The effects produced in iron at this exposure are relatively small compared to those observed in molybdenum and are most readily detected as changes in activation volume in the temperature range where the activation energy is changing most rapidly with stress, i.e., just below the point where dislocation motion ceases to be thermally activated. Measurements on Ferrovac-E showed that irradiation produced a decrease in activation volume from 183 b^3 to 120 b^3 at 295 °K, while in the zone-refined iron, where deformation is controlled by a different mechanism at this temperature, it increased the activation volume from 95 b^3 to 125 b^3.

There is a considerable controversy at the present time concerning the mechanism controlling dislocation motion in the temperature range from about 225 to 350 °K in iron. From these results it is evident that the controlling mechanism is different in Ferrovac-E and zone-refined iron and that the defects introduced by radiation either become the controlling barriers or modify the mechanism operative in the unirradiated material. These changes in activation volume are accompanied by an increase in shear stress at the lower yield point of 2.25 kg/mm^2 for Ferrovac-E and 1.76 kg/mm^2 for the zone-refined iron. Irradiation alters the temperature dependence of the

1. J. E. Dorn and S. Rajnak. Trans. Met. Soc. AIME, vol. 230, p. 1052. 1964.
2. F. A. Smidt, Jr. J. Appl. Phys., vol. 36, p. 2317. 1965.

flow stress only very slightly so the major part of these changes is due to an increase in the internal stress field which arises from long range interactions with the dislocations. Annealing these samples at 350 °C (0.35 T_m) for 3 hr, a treatment known to produce cluster growth and recovery of the mechanical properties in samples irradiated to higher exposures, produced a recovery of the yield stresses and a change in the activation volume of Ferrovac-E from 120 b^3 to 170 b^3 and for the zone-refined iron from 125 b^3 to 110 b^3.

The activation volumes of both Ferrovac-E and Battelle zone refined iron are observed to change as the deformation proceeds in the manner shown in Figure 3.8. The trend in both cases is for the activation volume of the irradiated samples to move toward those of the unirradiated samples as deformation progresses. This must mean that the dislocations are

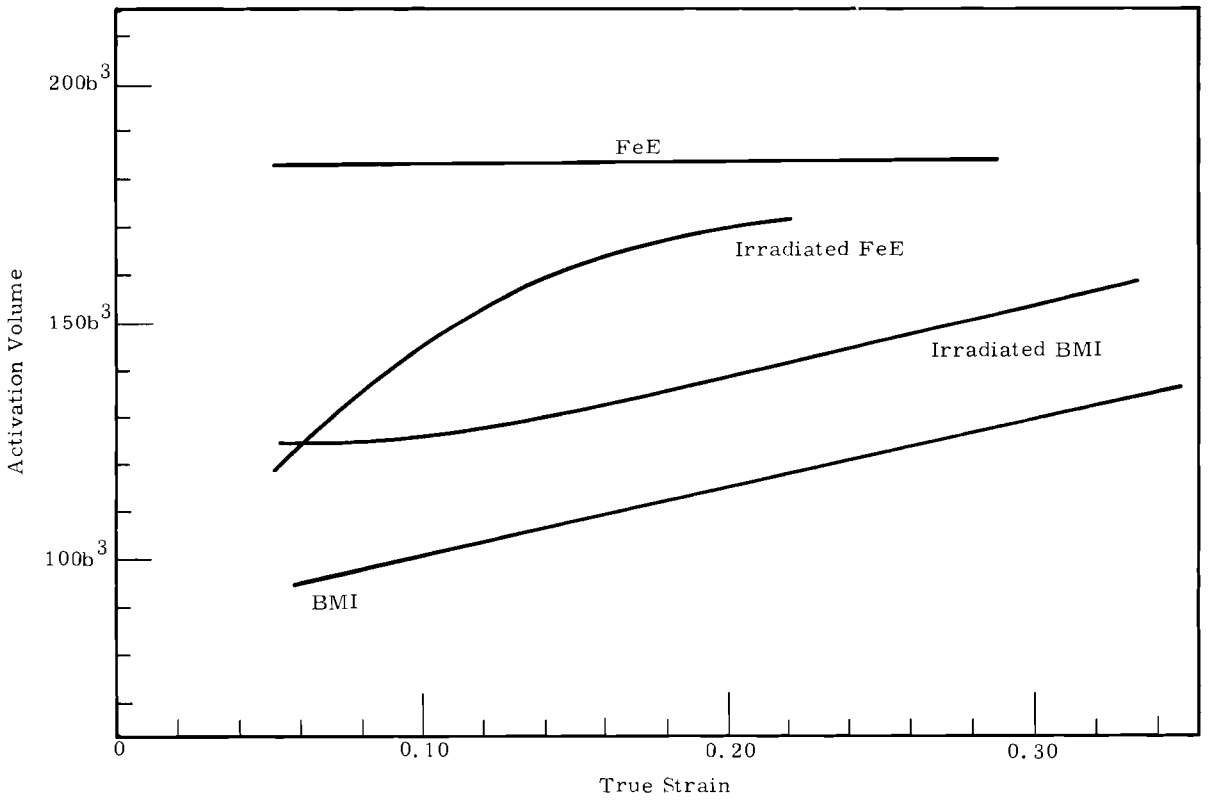

FIGURE 3.8

Variation of Activation Volume
with Strain in Polycrystalline Iron

interacting with the defects and removing them from the slip plane. If subsequent dislocations move through the same area rather than on planes not previously traversed their activation volumes would be expected to change in the direction of the control samples as observed. This is in accord with microscope observations of channeling and slip line studies which show that deformation in irradiated iron tends to take place by widening of already present glide bands rather than by frequent nucleation of new bands.

Molybdenum. Irradiation causes the activation volume of molybdenum to increase as in the case of zone refined iron and as shown in Figure 3.9, these apparent activation volumes converge with strain. The apparent volume at 50 °C (0.11 T_m) increases with strain from a value of about

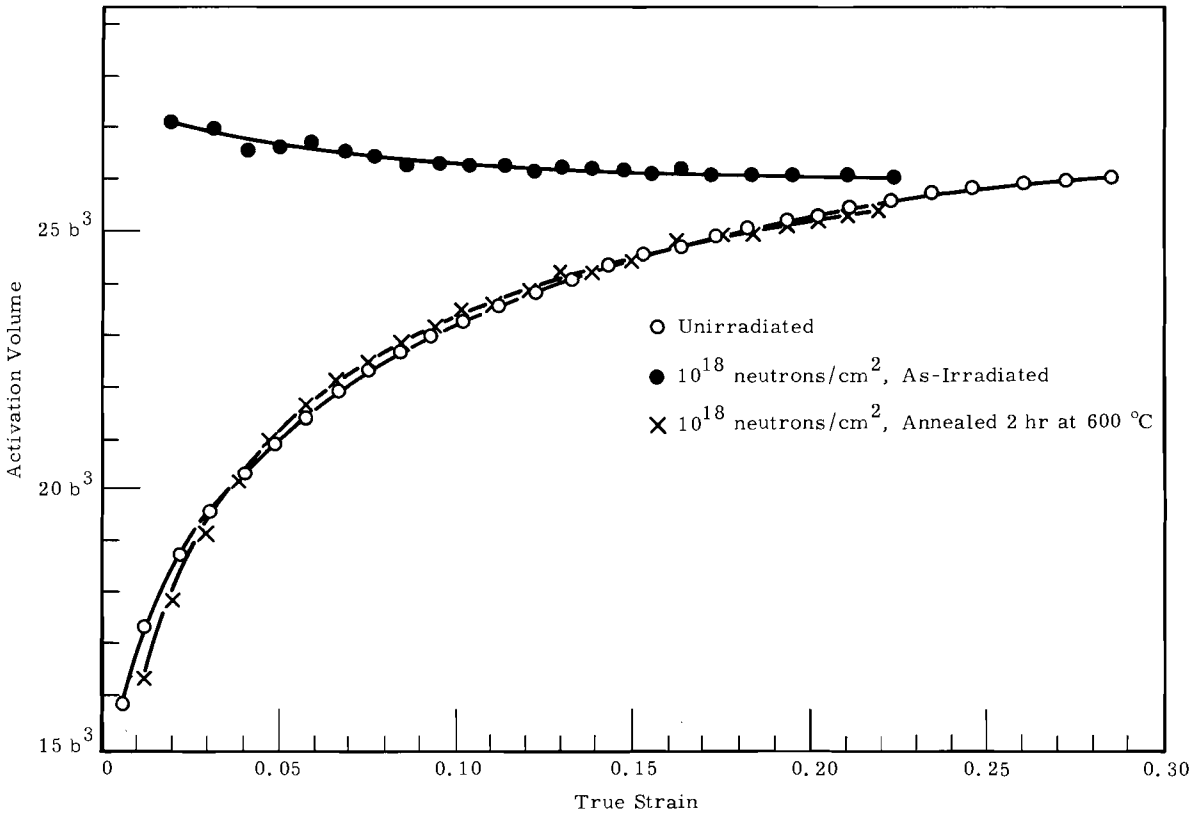

FIGURE 3.9

Variation of Activation Volume
with Strain in Polycrystalline Molybdenum

16 b^3 to about 26 b^3 at 30% strain for the unirradiated material. This range of values for the activation volume indicates that the rate-controlling process is the thermally-activated nucleation of kinks for overcoming the Peierls-Nabarro stress barrier. Other tests, to be reported elsewhere, confirm this conclusion.

The increase in V^* with strain is believed to be a consequence of a decrease in the athermal component of the applied stress with increasing strain, due to dislocation multiplication effects. Neutron irradiation causes an increase in V^* at low strains to a value of approximately 27 b^3; V^* then decreases with strain and approaches the unirradiated value. If the interaction between moving dislocations and the point defect clusters is the rate-controlling mechanism, then the activation volume should be of the order dba, where d is the mean cluster diameter and a the cluster spacing. However, for the observed concentration and size of defect clusters, the calculated value of V^* is almost three orders of magnitude greater than that determined experimentally, so that the visible defects are obviously not associated with the rate-controlling deformation process. If one assumes that there are some 10^{18} submicroscopic defect clusters per cm^3 and that these clusters have a mean diameter of 5 Å, the calculated value of V^* agrees closely with that observed. The return of the activation volume to the unirradiated value at higher strains must represent a gradual decrease in effectiveness of the small clusters as barriers to thermally-activated dislocation motion. Since the density of small clusters is high with respect to the large clusters and they have relatively small long-range stress fields, they will interact with dislocations in the initial stages of deformation and be removed. The two mechanisms may be thought to be superimposed and as the clusters are removed, the controlling mechanism in the unirradiated condition becomes dominant.

The activation volume of the irradiated material after annealing at 600 °C (0.3 T_m) returns to the unirradiated value. At this annealing temperature, the density of visible defects decreases slightly.[1] It is

---

1. B. Mastel and J. L. Brimhall. Acta Met., to be published.

reasonable to assume that the submicroscopic defects are being annihilated also, and possibly that they are removed at a greater rate. This is further evidence that the unresolvable defects are controlling the deformation mechanism.

Although channels have not been observed in molybdenum with an exposure of 10^{18} neutrons/cm^2, such a process may be occurring with respect to the submicroscopic defects. Sweeping up of the visible defects may not occur because the defects are not large enough to interact with dislocations moving on distant slip planes. With the spacing of defects observed at this exposure, 3×10^{-5} cm, the interaction distances are quite extended. Calculations based on those reported by Makin[1] show that a dislocation would have to be on a plane adjacent to the spot defect in order to result in an interaction.

Conclusions

Neutron irradiation of iron and molybdenum produces defects which may be seen with the electron microscope at exposures of 10^{18} neutrons/cm^2 in molybdenum and greater than 10^{19} neutrons/cm^2 in iron. Studies of thermally-activated deformation in these metals after irradiation demonstrate that submicroscopic defects are the obstacles which affect the thermally-activated motion of dislocations. Larger defects which are observed directly appear to contribute primarily to the long-range athermal stresses. The changes in activation volume during deformation of irradiated iron and molybdenum appear to be consistent with observations made by transmission electron microscopy, in that dislocation motion is confined to localized regions in the lattice. This localized deformation leads to the coarse slip traces, lower work hardening coefficient, and the reduction of uniform elongation without an accompanying decrease in reduction in area commonly observed in irradiated body centered cubic metals. In conclusion, it should be emphasized that neither of these experimental techniques is adequate in itself. The complimentary use of these two techniques will spur further progress toward a better understanding of deformation in irradiated materials.

---

1. M. J. Makin. The Long Range Forces Between Dislocation Loops and Dislocations, AERE R-4610, Atomic Energy Research Establishment, Harwell, Berkshire, England. May, 1964.

SWELLING OF IRRADIATED FISSIONABLE MATERIALS - J. L. Brimhall, R. D. Leggett, B. Mastel, K. R. Merckx, and H. A. Taylor

When fissionable metals are irradiated, the ordered metallic structure is perturbed in a number of ways. High energy neutrons and fission fragments collide with metal atoms, knocking them out of their structural positions. The resultant defects, vacancies, interstitials, dislocation loops, etc., can adversely affect metallic properties. Similarly, the fission products generated, some of which are noble gases, may be incompatible with the structure and so precipitate or coalesce as second phase inclusions or gas pores. Furthermore, the high localized temperatures associated with the fission event can cause anisotropic fissionable metals such as uranium to drastically change shape in accordance with the crystallography of the specimens.

These effects and their interactions are being studied with regard to the influence of irradiation variables such as the specimen temperature, burnup, burnup rate, and external pressure, and of metallurgical variables such as composition, structure, and geometry. The data thus far obtained on this program have established that, contrary to previous beliefs, swelling at low burnup in alpha uranium is due to mechanical processes associated with the irradiation "growth" phenomena and with fission event induced defects rather than the agglomeration and growth of fission gas pores. This is manifested as a maximum in the swelling temperature curve in the 400 to 600 °C range. Swelling continues to decrease above 600 °C up to about 700 °C. Above 700 °C, fission gas swelling begins to occur. A few tenths of a percent alloying addition or an applied external pressure have been found to be effective in overcoming this "mechanical" type of swelling. Efforts are continuing to better define the basic mechanisms involved and the interrelationships between burnup, temperature, pressure and metallurgical state. Fundamental information developed by this program will provide a basis for engineering exploitation of the many beneficial attributes of metal fuels for use in reactor applications.

Irradiation Program

A swelling capsule controlled at 450 °C and 500 psi reached a goal exposure and was discharged. A general swelling capsule was assembled and charged into a reactor and will operate at 30 psi to supply data on the effect of 0.1 at. % burnup and 700 °C (beta phase) temperature on the irradiation behavior of fissionable metals. Two controlled temperature-pressure capsules, assembled in tandem, were charged into a reactor and are operating successfully at respective control temperatures of 550 and 625 °C; a common source of pressurized helium maintains both capsules at 500 psi. The tandem arrangement permits efficient use of reactor space as well as an identical in-reactor experiment for more precise comparison of the effects of temperature and pressure. Each of the above capsules contains six high purity uranium, two U + Fe-Si, and two U + Fe-Al-Si half-tubular specimens having several heat treatments.

Construction was completed on a general swelling capsule to be irradiated at a control temperature of 700 °C at low pressure. This capsule will provide higher burnup data for high purity uranium irradiated in the beta and will permit evaluation of the influence of minor alloying additions on this behavior. Construction has begun on two swelling capsules which will be irradiated to high burnup. One capsule will be pressure-temperature controlled at 450 °C and 1000 psi; the other will operate at a controlled temperature of 450 °C without pressure restraint. The controlled pressure-temperature capsule, containing high purity and dilute alloy uranium specimens, will provide higher burnup data (~0.75 at. %) on the effect of external restraint. It will be recalled that at lower burnup (~0.13 at. %) the effectiveness with which pressure inhibited the swelling of high purity and alloy specimens was very marked.

Postirradiation Examination

Density measurements were completed on the specimens removed from Capsule P-4 irradiated at 625 °C and 1000 psi to 0.2 at. % burnup. Optical and electron metallography are partially completed. Table 3.3 summarizes the metallurgical and irradiation histories and the observed

TABLE 3.3

SWELLING OF SPECIMENS IN CAPSULE P-4 IRRADIATED AT 625 °C AND 1000 psi TO 0.2 at. % BURNUP

Specimen Number	Type Material*	Heat Treatment	Irradiation Temperature, °C Reactor Power Full	Irradiation Temperature, °C Reactor Power Zero	As Irradiated ρ_f g/cc	% Swelling $\frac{\rho_i - \rho_f}{\rho_f} \times 100$	"R" = % Swelling/ at. % Burnup	"R" for Comparable Specimen Irradiated at 20 psi
A-1	T-3	As-extruded	520	≃345	15.96	19.2	96	400
A-2	T-3	As-extruded	520	≃345	18.31	3.5	17	400
B-1	A	Beta quenched in the bulk prior to specimen machining	590	≃415	18.83	0	0	10
B-2	A	730 °C - 15 min - oil quenched	590	≃415	18.67	0.9	5	10
C-1	T-3	As-extruded	625	≃450	18.57	2.5	13	60
C-2	T-3	As-extruded	625	≃450	18.71	1.7	9	60
D-1	T-3	730 °C - 15 min - oil quenched	620	≃450	18.70	1.5	8	60
D-2	T-3	730 °C - 15 min - oil quenched	620	≃450	18.85	0.5	3	60
E-1	B	Beta quenched in the bulk prior to specimen machining	585	≃415	18.45	2.2	11	50
E-2	B	Beta quenched in the bulk prior to specimen machining 730 °C - 15 min - furnace cooled; 730 °C - 15 min - oil quenched	585	≃415	18.75	1.1	5	50

* T-3: High Purity Uranium - 65 ppm Fe, <5 ppm Al, 24 ppm Si, 6 ppm C.
A: U + Fe-Al-Si Alloy - 400 ppm Fe, 640 ppm Al, 85 ppm Si, 500 ppm C.
B: U + Fe-Si-Alloy - 140 ppm Fe, ≃25 ppm Al, 95 ppm Si, 400 ppm C.

swelling in the 10 specimens contained in this capsule. The swelling that was observed in similar specimens irradiated at about 20 psi in low pressure capsules is also included. The 1000 psi pressure is effective in reducing the amount of swelling observed in high purity uranium irradiated at low pressure by a factor of 5 to 20. In the U + Fe-Si alloy, the reduction factor was 5 to 10 and in the U + Fe-Al-Si alloy, the factor was about 2.

Metallographic examination revealed structures very similar to those observed after irradiation at low pressures except that the magnitude of the porosity is substantially less in agreement with the density measurements. Figure 3.10 shows the structure of the as-extruded high purity uranium specimen. Large tears are prevalent at the grain boundaries and tiny matrix pores are distributed throughout the grains. The matrix porosity is shown in Figure 3.11.

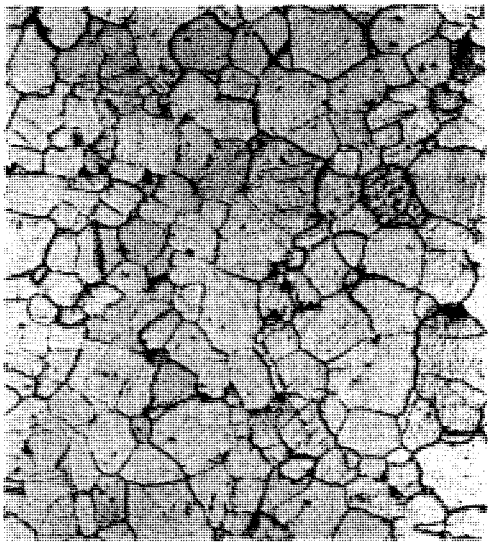

250X

1000X

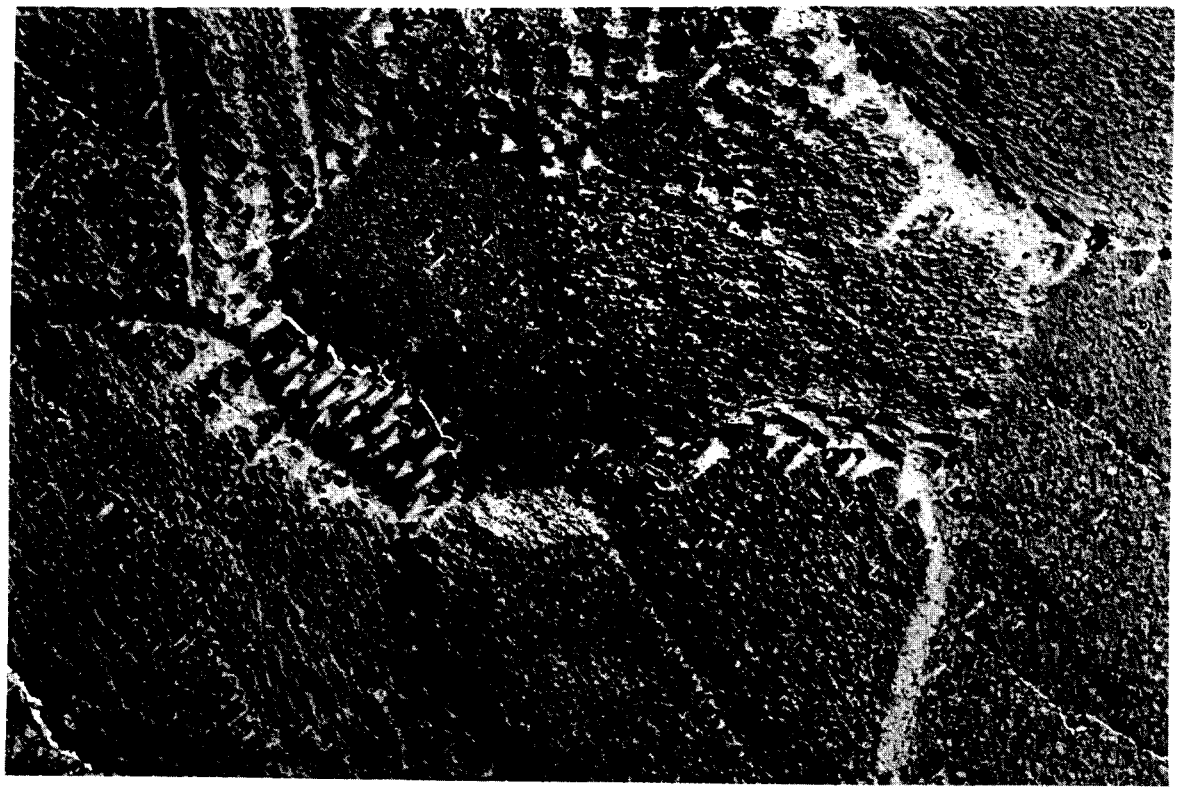

3500X

FIGURE 3.10

As-Extruded High Purity Uranium Specimen P-4 C-1
Irradiated at 625 °C and 1000 psi to 0.2 at. % Burnup

Neg. D-1116, D-1119, 3394D

15,000X

FIGURE 3.11

As-Extruded High Purity Uranium Specimen P-4 C-1
Irradiated at 625 °C and 1000 psi to 0.2 at. % Burnup

Neg. 3395D

REACTOR METALS RESEARCH UNIT

IN-REACTOR MEASUREMENTS OF MECHANICAL PROPERTIES -

J. A. Williams, D. H. Nyman, and J. W. Carter

The purpose of in-reactor measurements is to determine the effects of fast neutron irradiation on the mechanical properties of structural materials. In-reactor creep measurements are currently being conducted on annealed 304 SS and annealed Zircaloy-2. Creep-rupture studies of Hastelloy X at high temperature are continuing.

In-Reactor Creep

In-reactor and out-of-reactor creep rates of 3.3 and 2.5 x 10^{-6}/hr, respectively, were measured for annealed 304 SS after 2500 hr of testing at 550 °C and 30,000 psi stress. The in-reactor test was terminated by specimen failure after 2838 hr. This value represents a reduction of creep-rupture life since the unirradiated control is still in progress after 4000 hr of testing.

The creep rate measured in-reactor for annealed Zircaloy-2, tested at 315 °C and 15,000 psi, is on the order of 1 to 4 x 10^{-7}/hr. This rate was determined after 1000 hr of testing during which time considerable power fluctuations in the PRTR were encountered. No significant differences in creep rates during reactor outages as compared to reactor operating periods were observed. The creep rate of the out-of-reactor control test was 1.9 x 10^{-7}/hr. It might well be assumed that at the conditions of this test there is little effect of irradiation on the creep of annealed Zircaloy-2.

High Temperature Creep-Rupture Tests

Five creep-rupture tests on Hastelloy X have been completed at a temperature of 1950 °F. These results are given in Table 4.1, along with results previously obtained at 2100 °F. Figures 4.1 and 4.2 show these results compared with lower temperature data determined by other investigators.(1)

---

1. M. J. Donachie and R. G. Shepheard. Materials Research and Standards, p. 495. September, 1960.

TABLE 4.1

CREEP-RUPTURE RESULTS OF HASTELLOY X

Temperature, °F	Stress, psi	Minimum Creep Rate, hr	Elongation, %	Time To Rupture, hr
1950	8000	3.0×10^{-1}	27.0	0.7
	6000	1.5×10^{-1}	32.9	3.9
	4000	3.2×10^{-2}	26.5	7.3
	2500	4.8×10^{-3}	19.0	36.0
	1500	1.3×10^{-3}	24.1	250.0
2100	5000	4.8×10^{-1}	24.7	0.4
	4000	3.0×10^{-1}	23.5	0.6
	3000	1.1×10^{-1}	23.4	2.0
	2500	3.1×10^{-2}	19.8	4.3
	1300	7.7×10^{-3}	23.0	21.0
	900	1.4×10^{-3}	10.8	65.0
	500	7.2×10^{-4}	14.2	114.5
	300	2.0×10^{-4}	14.2	340.0

The low stress, high temperature creep rupture behavior of this alloy in vacuum is similar to the results on nickel-base alloys reported by other investigators.[1-5]

1. M. J. Donachie and R. G. Shepheard. Materials Research and Standards, p. 495. September, 1960.
2. P. Shahinian and M. Achter. ASM Transactions, vol. 51, p. 244. 1959.
3. P. Shahinian and M. Achter. AIME Transactions, vol. 215, p. 37. 1958.
4. P. Shahinian and M. Achter. ASM Transactions, vol. 49, p. 862. 1957.
5. R. Widmer and N. Grant. ASME Transactions, vol. 82, p. 882. 1960.

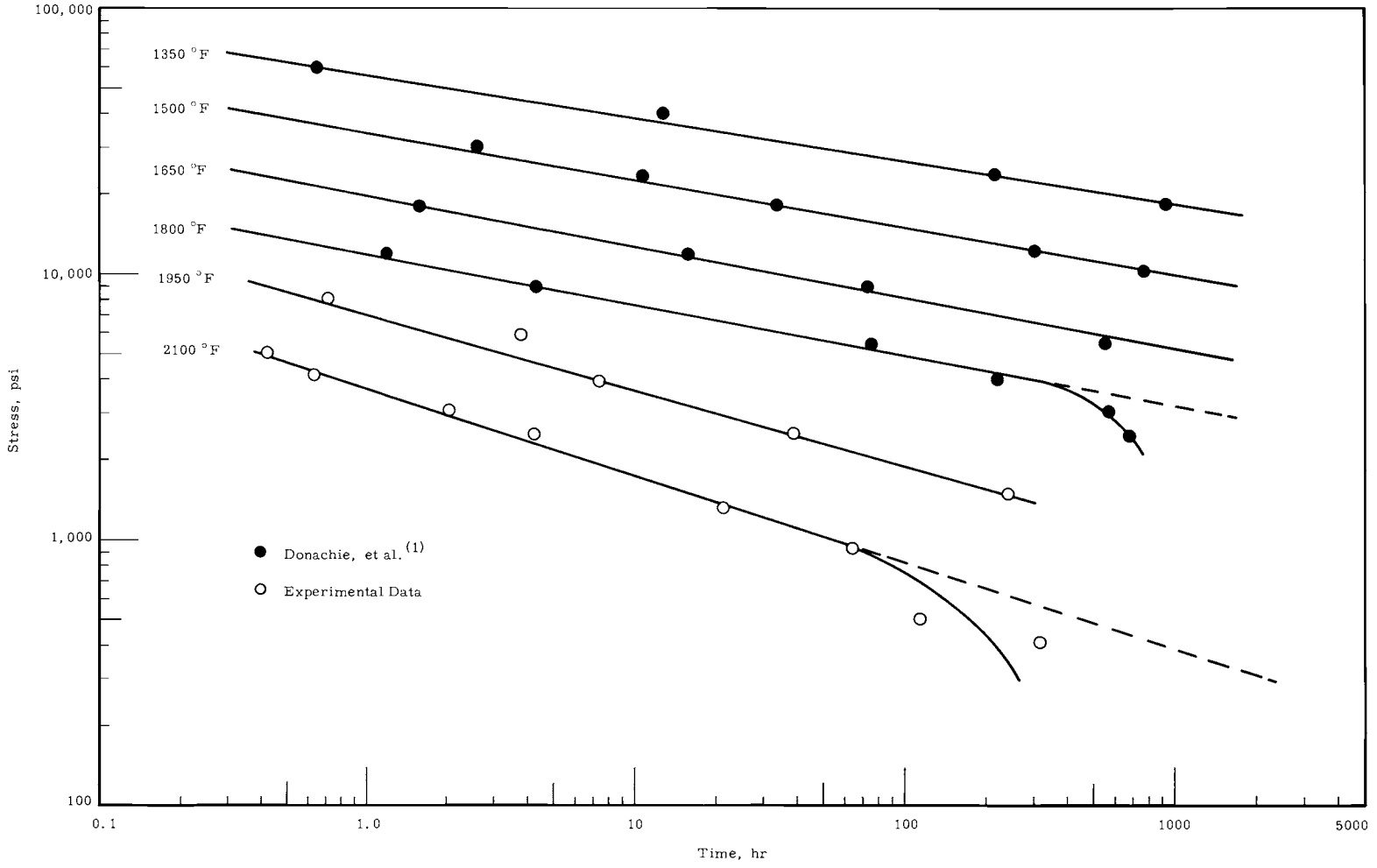

FIGURE 4.1
Stress-Rupture Data for Hastelloy X

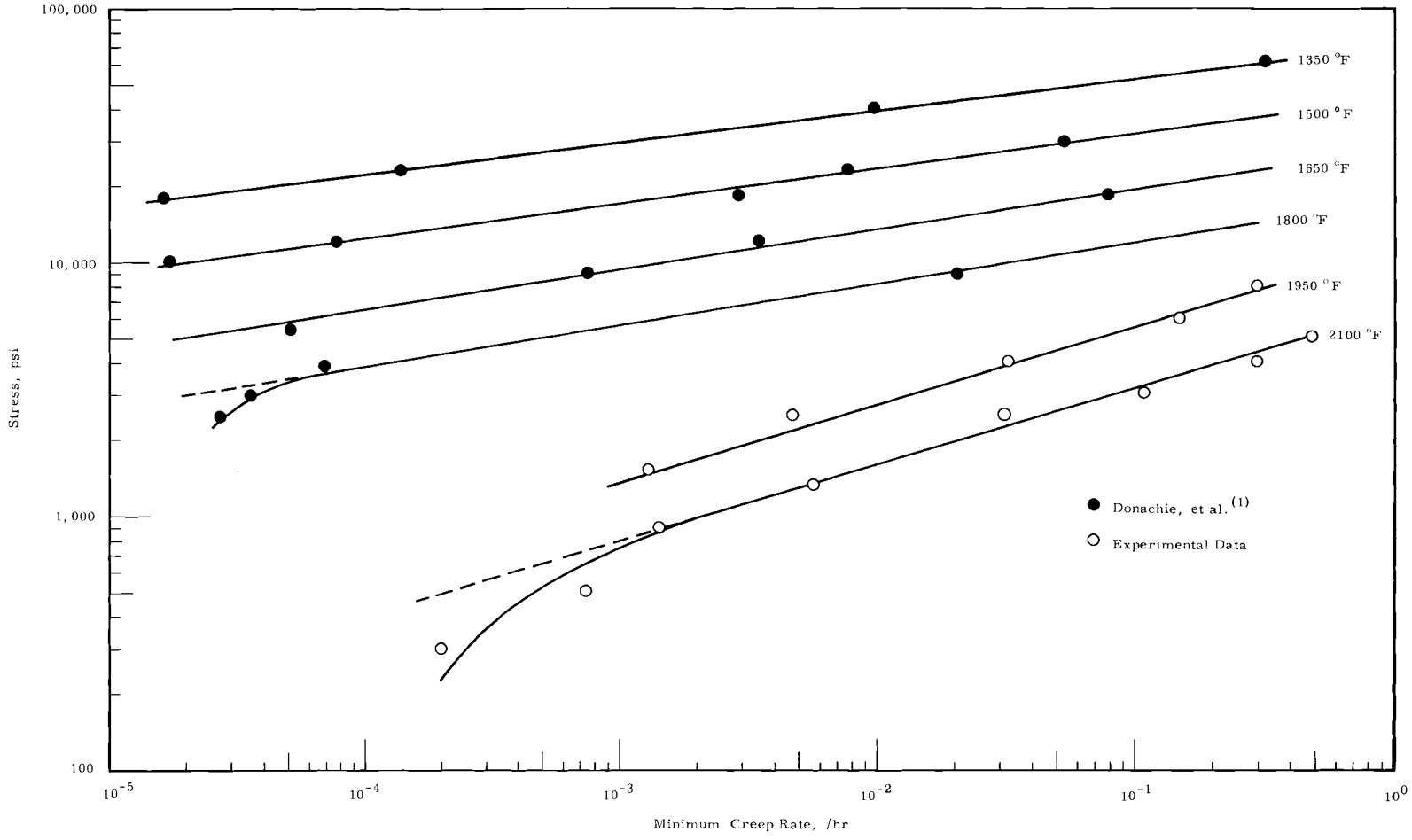

FIGURE 4.2

Stress Versus Minimum Creep Rate for Hastelloy X

Shahinian and Achter's[1, 2] proposed explanation of environmental creep-rupture effects can be used to account for this behavior. Their work showed that Nichrome V and nickel had better rupture strength in air at low stress while at high stress the reverse was true, i.e., higher rupture strength in vacuum. This was explained on the basis of two competing processes, (1) oxidation strengthening and (2) reduction in strength due to a a lowering of the surface energy. Air strengthening can be due to one or more processes. Surface oxidation may act as a barrier to dislocations while internal oxidation reduces the stress concentration by blunting a crack tip. Surface energy effects due to gas adsorption do not play a major role in this investigation since the tests were carried out in vacuum at pressures to 5×10^{-5} Torr.

At low stresses and high temperatures, a definite deviation from a power law relationship appeared for both rupture life and minimum creep rate, Figures 4.1 and 4.2. Additional low stress tests are being run at 1950 °F to determine the extent of the curve. Similar downward deviations have also been noted by Donachie and Shepheard.[3] They assumed that vacuum data represented the intrinsic strength of the alloy; therefore, the downward break in vacuum data results from the lack of air strengthening.

In this investigation, however, the reduced rupture life and increased creep rate at low stresses can be explained in terms of grain growth and its influence on intergranular crack propagation. Referring to Table 4.1 and Figure 4.3, it can be seen that for stresses above 1300 psi at 2100 °F, the rupture times are relatively short, i.e., less than 21 hr, and values of total elongation at rupture vary from 19.8 to 24.7%. The microstructures are similar in that there is very little grain growth and many intergranular

---

1. P. Shahinian and M. Achter. ASM Transactions, vol. 51, p. 244. 1959.
2. P. Shahinian and M. Achter. AIME Transactions, vol. 215, p. 37. 1958.
3. M. J. Donachie and R. G. Shepheard. Materials Research and Standards, p. 495. September, 1960.

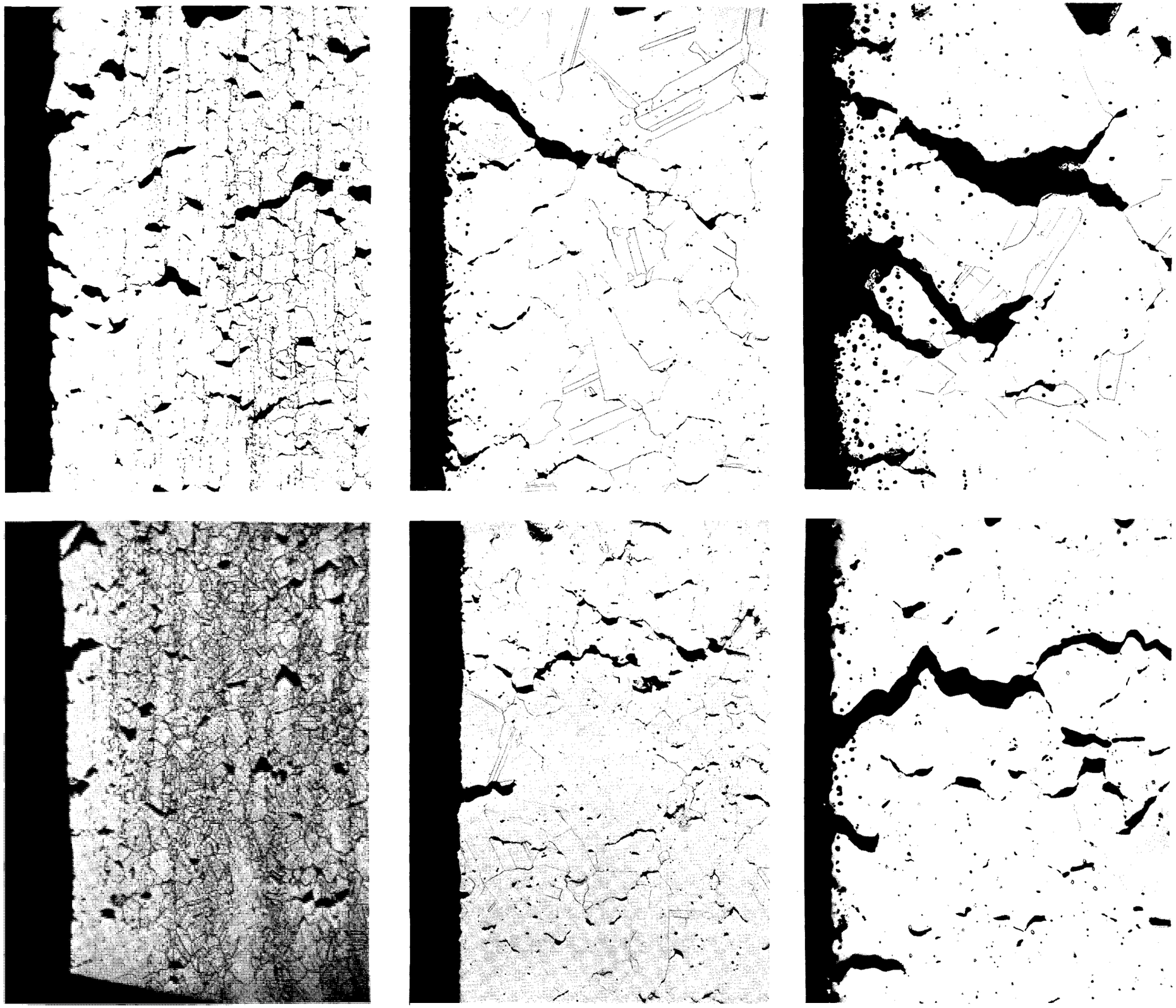

FIGURE 4.3
Mode of Fracture Initiation in Vacuum at 2100 °F

cavities. At stresses below 1300 psi the rupture times are much longer and values of total elongation are reduced almost 50%. The microstructure shows considerable grain growth, a lack of second phase, large cracks extending to the surface, and subsurface voids.

The subsurface voids are attributed to the volatilization of manganese and chromium, which have a vapor pressure of 5×10^{-1} Torr and 1.2×10^{-4} Torr, respectively at 2100 °F. The formation of these voids is time-dependent as seen in Figures 4.3d, 4.3e, and 4.3f. At longer times, the voids are present at greater depths below the surface.

The larger grains resulting from grain growth have much less grain boundary area for supporting plastic deformation of the specimen by grain boundary shear, and rupture occurs prematurely. Although measured minimum creep rates appear to be greater than extrapolated values for the large-grained material, the lack of structural stability during the test renders those values nonrepresentative of the final grain size.

WELD ZONE FRACTURE TOUGHNESS DETERMINATIONS -

R. G. Hoagland and R. G. Rowe

Recent tests were performed to determine the fracture toughness of welded ASTM A302-B steel. Double cantilever beam (DCB) specimens were machined from a 1 in. plate of A302-B steel containing a double-bevel butt weld. The welding procedure is described in Figure 4.4. The specimens were machined from the mid-thickness of the plate with their length lying perpendicular to the weld. It was thus possible to obtain a fracture toughness profile through both the welded and heat affected zones.

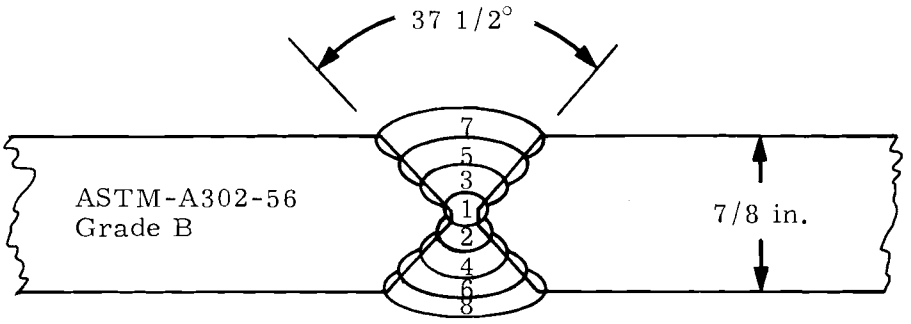

Welding Process	-	Shielded Metal Arc
Position of Welding	-	Flat (plate turned to permit flat position welding)
Welding Electrodes	-	E10016 (AIRCO 394)
Preheat	-	None
Postheat	-	None
Amperes	-	Pass No. 1 - 150 Passes No. 2 through 8 - 180
Volts	-	20

Back side of Pass No. 1 was ground prior to deposition of Pass No. 2

FIGURE 4.4

Welding Procedure Used for Test Weld on ASTM A302-B Plate

Due to the high toughness of A302-B steel, it was necessary to increase the width of the DCB specimen to 1/2 in. to provide sufficient elastic restraint to measure plane strain toughness data. The strain energy release rate was calculated from the equation

$$G_{Ic} = \frac{Ey^2 m}{2BW} \left(\frac{Bf}{Ey}\right)^{\frac{M+1}{m}}$$

where $E = 29.6 \times 10^6$ psi

$m = 2.733$

$B = 304$

f = load

y = extension

B and m are constants dependent upon the geometry of the DCB specimen and E is Young's modulus.

The dimensions of the specimen were:

height = 1.000 in.
gross beam width = 0.500 in.
net beam width = 0.140 in.
length = 7.0 in.

After welding and machining, the specimens were austenitized at 1750 °F for 1/2 hr and water quenched. Specimen WA3-2 was tested in the as-quenched condition, and specimen WA3-4 was stress relieved at 600 °F for 1/2 hr and air cooled before testing. All fracture toughness data were taken at room temperature (22.5 °C).

The results of these tests are shown in Figure 4.5. The two upper curves are plots of G_{Ic} (WA3-2 represented by triangle, and WA3-4 represented by circles) and the lower curve is the hardness profile of specimen WA3-2.

These tests indicate a maximum toughness in the filler metal with a region of minimum toughness immediately adjacent to it. A second toughness maximum is observed in the heat affected zone with the toughness

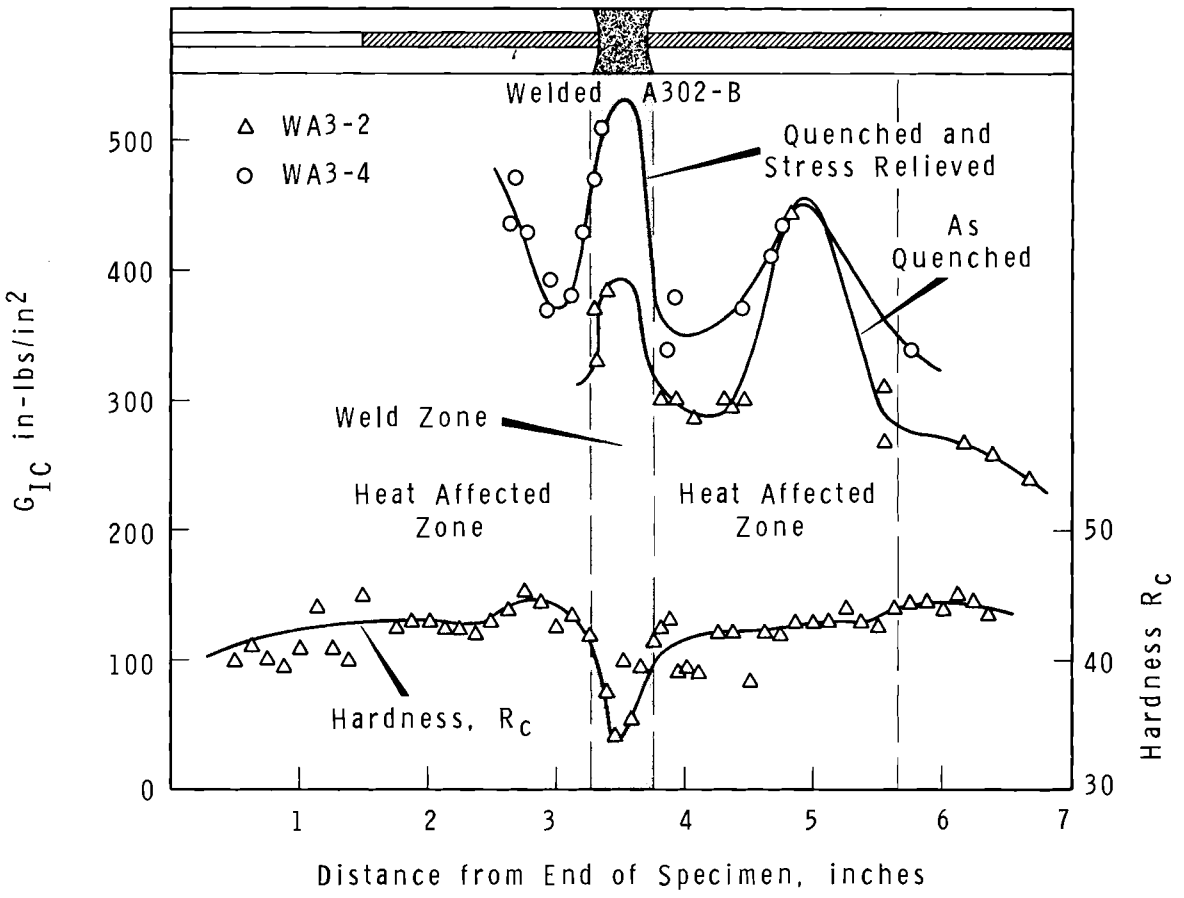

FIGURE 4.5

Variation of Fracture Toughness Through the Weld Zone

slowly decreasing to a constant value in the base metal. The hardness profile shows correspondence with the maximum toughness region in the filler metal but there is a striking difference in the hardness profile and the G_{Ic} curve in the region corresponding to the toughness maximum in the heat affected zone. This points out that the fracture toughness is not directly related to the hardness, but is more sensitive to the microstructure of the material.

It was also noted that the stress relief heat treatment had less effect upon the heat affected zone than the weld zone, indicating that the microstructure in this zone has a stronger influence on fracture toughness than do residual stresses.

The nature of the fracture toughness profile obtained indicates that three factors affecting the toughness are (1) the grain size, (2) the amount of stable carbide precipitates present, and (3) the phases present in the microstructure. Metallographic investigations are underway to determine the exact relationship between the fracture toughness, the hardness, and the microstructure.

These preliminary tests demonstrate the usefulness of the DCB specimen in examining the fracture toughness of a welded material. With a single DCB specimen it is possible to determine the entire toughness profile across the weld. The effect of various heat treatments can readily be observed due to (1) the sensitivity of the method to changes in the microstructure, and (2) the ease with which the tests may be performed. Further tests are soon to be underway to ascertain the effect of both preweld and postweld heat treatments.

CHEMICAL METALLURGY UNIT

ATR GAS LOOP SUPPORT

Corrosion Studies - L. A. Charlot and R. E Westerman

The oxide films formed on the superalloys Haynes Alloy 25 and Hastelloy X-280 have been examined in thermal cycling tests under severe oxidizing conditions,[1] in isothermal oxidation tests followed by evaporation at test temperature[2] and in low partial pressure oxidant tests at constant temperature.[3] The premise held during this work was that a thin oxide film formed on these alloys either by preoxidizing or normal oxidation during Advanced Test Reactor (ATR) operation would be beneficial in impeding metal evaporation. Previous tests showed that evaporation can be retarded by oxide formation, but that the oxide films formed were not, in every case, completely protective. To add additional information to oxide film mechanics, another series of tests using prefilming as a parameter was run.

Samples of Haynes Alloy 25, Hastelloy X-280 and Nichrome were prepared for the oxide adherence study by abrasion on a 400X grit belt. The samples were weighed, then oxidized at 2050 °F in air for 4, 15, 60, and 240 min. The oxidized samples were then exposed to vacuum conditions ($\sim 10^{-4}$ Torr) at 2050 °F for 24 hr. The vacuum was imposed to simulate ATR loop exposure to ultrapure helium.

The preoxidation did not result in formation of a protective film on any alloy tested. All samples showed loss of the oxide film (and probably concurrent metal evaporation) during the vacuum treatment, ranging from

---

(1) Quarterly Progress Report, Metallurgy Research Operation, October, November, December, 1964, edited by J. J. Cadwell, HW-84573. General Electric Company, Richland, Washington. January 15, 1965.

(2) Quarterly Progress Report, Metallurgy Research Operation, January, February, March, 1965, edited by J. J. Cadwell, BNWL-79. April 15, 1965.

(3) Quarterly Progress Report, Metallurgy Research Operation, April, May, June, 1965, edited by J. J. Cadwell, BNWL-120. July 15, 1965.

complete oxide loss (mirror shiny sample) to exposure of about 50% of the metal substrate. All samples showed a net weight loss after oxidation and vacuum treatment. The Nichrome samples were prone to oxide spallation even before the vacuum treatment, while the Hastelloy X-280 and Haynes Alloy 25 showed reasonably good oxide retention after the short oxidation treatments employed.

From a weight loss analysis and also visual inspection of the oxide films after these tests, prefilming does not yield an adherent, protective, evaporation barrier. Any oxide on the sample will impede metal loss by evaporation; however, oxide degradation by thermal cycling (mechanical spalling of the film) or exposure to nonreactive atmospheres (inert gas or vacuum) will permit only limited protection by the oxide film.

Dynamic Materials Test Apparatus - R. A. Thiede and R. E. Westerman

The burned-out platinum preheater has been replaced in the DMTA, and several successful superalloy evaporation experiments have been recently conducted. The zirconium getter bed maintains the purity of the helium gas at a sufficiently high level to prevent sample oxidation.

The evaporation experiments conducted so far have utilized a helium gas temperature of 2050 °F (at the test section), a helium gas pressure of about 350 psig, and Hastelloy samples. The gas flow rate is the primary variable under consideration. The results of the evaporation are summarized in Table 5.1.

TABLE 5.1

EVAPORATION OF HASTELLOY-X AT 2050 °F IN PRESSURIZED FLOWING HELIUM

Sample	Linear Helium Flow Rate, ft/sec	System Pressure, psig	Test Duration, hr	Weight Loss, $mg/cm^2/day$
5	490	340-357	76-1/2	1.20
8-1	490	362-365	73	0.89
8-2	196	349-363	94-1/2	0.52
8-3	98	350-360	80-1/2	0.45

These preliminary data indicate that evaporation rates of Hastelloy X in pressurized flowing helium are considerably less than the evaporation rate found in high vacuum conditions at the same temperature, namely ~3.8 $mg/cm^2/day$. Furthermore, it appears that the evaporation rates may be roughly proportional to the helium flow rate. Tests are in progress to determine more precisely the relation of evaporation rates to flow.

PRODUCTION REACTOR CORROSION AND COATINGS STUDIES

Hydrogen Pickup of Zircaloy in Low Temperature Water - R. L. Dillon and B. Griggs

The introduction of hydrogen into Zircaloy during low temperature exposure to moist hydrogen previously reported[1] suggested a more general inquiry into the conditions for low temperature hydriding of zirconium alloys. The following describes additional studies in hydrogen saturated water and the effects of applied potentials and galvanic coupling of Zircaloy to aluminum.

Pickup of Hydrogen by Zirconium Exposed in Hydrogenated Process Water

Zircaloy-2 samples taken from the hydrogenated water experiment after 4 mo were analyzed for hydrogen. Zircaloy-2 samples were present in the test both coupled to 8001 and uncoupled, with, however, the possibility that random contact of Zircaloy samples to aluminum may have occurred. The results of this experiment are shown in Table 5.2.

TABLE 5.2

HYDROGEN PICKUP IN HYDROGENATED WATER
90 °C, pH 6.6 PROCESS WATER,
H_2 BUBBLED THROUGH SYSTEM FOR 132 DAYS

Sample	Hydrogen Analysis*
Etched Zircaloy-2	32 ppm
Vapor-blasted Zircaloy-2	32 ppm
Vapor-blasted Zircaloy-2 coupled to X-8001	51 ppm

* Blank hydrogen analysis for this sample stock ~20 ppm.

The rates of pickup of hydrogen in this experiment are relatively slow when coupling to aluminum is casual or nonexistent. The hydrogen pickup for the specimen coupled to X-8001 is reasonably consistent with

(1) Quarterly Progress Report, Metallurgy Research Operation, January, February, March, 1965, edited by J. J. Cadwell, BNWL-79. April 15, 1965.

the data of Table 5.5. Without the agency of hydrogen discharge at the cathodic Zircaloy-2 surface, the hydriding process in hydrogenated water appears slow.

Hydrogen Charging by Applied Potentials

Table 5.3 summarizes the effects of 0.5, 1.5, 3.0, and 4.5 cathodic potentials (-) applied to Zircaloy-2 coupons exposed in 90 °C pH 6.6 process water for periods up to 2000 hr. The results are reported

TABLE 5.3

HYDROGEN PICKUP IN ZIRCALOY-2 CATHODES AS A FUNCTION OF APPLIED VOLTAGE AND TIME*

Time, hr	0.5 V	1.5 V	3.0 V	4.5 V
138	25,28	28,33	413,387	916,807
377	27,27	34,33	1,225	1,702
815	33,37	43,43	1,611	2,052
1,983	50,53	88,88	3,578	4,119

* pH 6.6, process water electrolyte at 90 °C preexposure hydrogen concentrate of sample stock ~20 ppm.

in terms of the total hydrogen analyzed in the Zircaloy-2 by hot vacuum extraction. Blank hydrogen in the unexposed sample stock is about 20 ppm. It is apparent from these results, which, by the way, are confirmed by metallography, that potentials as low as 0.5 V are capable of introducing hydrogen into zirconium alloys. A sidelight of these data is the calculation of the efficiency of the hydriding process based on current flow between the zirconium cathode and stainless steel anode, Table 5.4. The efficiency

TABLE 5.4

EFFICIENCY RATIO (R_c) FOR HYDRIDING PROCESS*

Time, hr	0.5 V	1.5 V	3.0 V	4.5 V
138	1.90	0.330	0.070	0.073
377	0.90	0.130	0.130	0.057
815	0.91	0.054	0.077	0.030
1983	1.10	0.071	0.073	0.026

* $R_c = \frac{\text{Equivalents of Hydrogen Absorbed}}{\text{Equivalents of Current Passed}}$

of the low voltage system (0.5 V) is significantly greater than the 1.5, 3.0, and 4.5 V systems. The differences among the latter three systems are possibly not significant in view of the approximate nature of the calculations.

Hydrogen Charging in Galvanically Coupled Zircaloy-2

Galvanic potentials and currents established between Zircaloy and aluminum in pH 6.6, 90 °C process water vary with time and aluminum alloy. Values at 1008 hr are shown in Table 5.5. It is of some interest

TABLE 5.5

HYDROGEN ANALYSIS OF ZIRCALOY-2 GALVANICALLY COUPLED TO X-8001 AND 6063 ALLOYS IN 90 °C PROCESS WATER pH 6.6

Time, hr	Zircaloy-2 6063 Al	Zircaloy-2 X-8001
1008	65 to 75 ppm*	33 to 40 ppm*

* Blank hydrogen analysis of sample stock ~20 ppm.

that the amount of hydrogen introduced into the Zircaloy-2 is dependent on the aluminum alloy to which it is coupled. Approximately three times as much hydrogen was absorbed by the Zircaloy-2 sample bolted to 6063 alloy (Al–0.7 Mg–0.4 Si) as the sample bolted to 8001 (Al–1% Ni–0.5% Fe). Presumably these differences result from the local cathodes (Al, Ni, Fe intermetallic phases) present in the 8001 alloy.

Effect of ac Potentials on the Hydriding Process

In one experiment two aluminum alloy coupons and an abraded Zircaloy-2 coupon in 90 to 100 °C process water were charged with a 3 V (rms) 60 cycle potential from an autotransformer for 24 hr. Hydrogen analysis of Zircaloy coupons was 92 ppm (blank analyses $\approx$20 ppm H_2). A subsequent experiment utilizing as-received Zircaloy-2 sheet and coupons of several different metals (304 SS, 6063 and 8001 aluminum, platinum, and Zircaloy-2) for a similar time in 85 to 90 °C process water showed little, if any, hydrogen pickup. These coupons were separately charged with 3 V (rms) 60 cycle potential from separate standard stepdown transformers. The differences between these experiments are currently under investigation.

N-REACTOR CORROSION AND HYDRIDING STUDIES

Effects of Vacuum Annealing on the Oxidation of Prefilmed Zircaloy-2 -

A. B. Johnson, Jr.

Several investigators[1-4] have found that a sufficiently severe vacuum anneal of oxidized zirconium and Zircaloy causes loss of the protective character of the oxide. Previous work[5] at this laboratory on vacuum annealing effects on Zircaloy-2 and zirconium showed that at a critical thickness of oxide dissolution (~1500 to 2000 Å), the protective character of the oxide deteriorated. The postanneal oxidation rate then increased with increasing severity of anneal to complete dissolution of the oxide. Subsequent to vacuum anneals calculated to completely dissolve the oxide (6, 10, 20, 35 mg/dm^2 oxide thicknesses), the postanneal oxidation was accelerated, but returned to normal. However, on one set of coupons annealed well beyond the point of complete dissolution, the postanneal oxidation rate began rapidly, diminished and then underwent transition to a markedly accelerated rate 20 to 30 days after the anneal.

However, the anneals were performed in an ungettered system. Wanklyn[6] has shown that silicon contamination from anneals in quartz

---

(1) R. D. Misch and F. H. Gunzel, Jr. "The Electrical Resistance of Oxide Films on Zirconium in Relation to Corrosion," J. Electrochem. Soc., vol. 1, p. 15. 1959.

(2) S. Kass and D. B. Scott. Effect of Partial Dissolution of the Oxide Film on the Aqueous Corrosion Resistance of Zircaloy-2, WAPD-T-1078. Westinghouse Electric Corporation. October, 1959. Also in J. Electrochem. Soc., vol. 109, pp. 92-94.

(3) C. L. Crenshaw and A. M. Andrako. The Effects of Annealing on the Corrosion Rate of Pre-Oxidized Zircaloy-2, KAPL-M-AA-4. Knolls Atomic Power Laboratory, November 1962.

(4) B. Cox. Some Factors Which Affect the Rate of Oxidation and Hydrogen Absorption of Zircaloy-2 in Steam, AERE-R-4348. United Kingdom Atomic Energy Authority. July, 1963.

(5) A. B. Johnson, Jr. "Oxidation of Zirconium and Zircaloy-2 Following Vacuum Annealing of Autoclaved Oxide Films," paper presented at the Electrochemical Society Meeting, Washington D.C. October 11-15, 1965.

(6) J. N. Wanklyn. Unpublished Data. Atomic Energy Research Establishment, Harwell, England. (Personal Communication)

causes accelerated oxidation of zirconium. A set of anneals therefore was undertaken in which a Zircaloy-2 coupon was enclosed in a Zircaloy-2 foil (thickness 5 mils); other Zircaloy-2 coupons were suspended outside the foil, in the same anneal. The system was pumped down to $< 10^{-5}$ Torr prior to the anneal. Anneals were performed at 700 °C for 370 min and at 800 °C for 70 min. The times were at least twice as long as those calculated to give complete dissolution of the 20 mg/dm^2 oxides.

Effects of the anneals on the postanneal oxidation behavior are shown in Figure 5.1. The enclosed and unenclosed samples at both temperatures showed immediate accelerated postanneal oxidation, followed by a second, more pronounced acceleration 15 to 25 days after the anneal. The 700 °C samples show the beginning of a third acceleration 50 to 55 days after the anneal.

Since samples inside and outside of the foil showed no essential differences in postanneal oxidation behavior, surface contamination during the anneal is not the explanation for the accelerated attack.

A coupon annealed at 700 °C, outside the foil, was etched to remove ~3000 Å of the annealed surface (calculated from weight loss due to etching). Etching eliminated the first accelerated attack (Figure 5.1), but the second acceleration occurred as for the unetched coupons.

It is postulated that the annealed surface is either highly stressed or porous (capacitance measurements favor the latter). Removal of the annealed surface by etching precluded the initial rapid attack.

In previous runs, for coupons annealed to give oxygen penetrations of ~2 to 3 x 10^{-4} cm ($\sqrt{Dt}$), multiple transitions were relatively small or absent. Only for oxygen penetrations of > 6 x 10^{-4} cm did the marked acceleration occur. This suggests that the second acceleration is related to the creation of an oxygen-rich metal layer of some critical thickness. One coupon sectioned at 44 days (total exposure), during the second transition, showed cracks extending to the bottom of the oxygen-rich metal layer

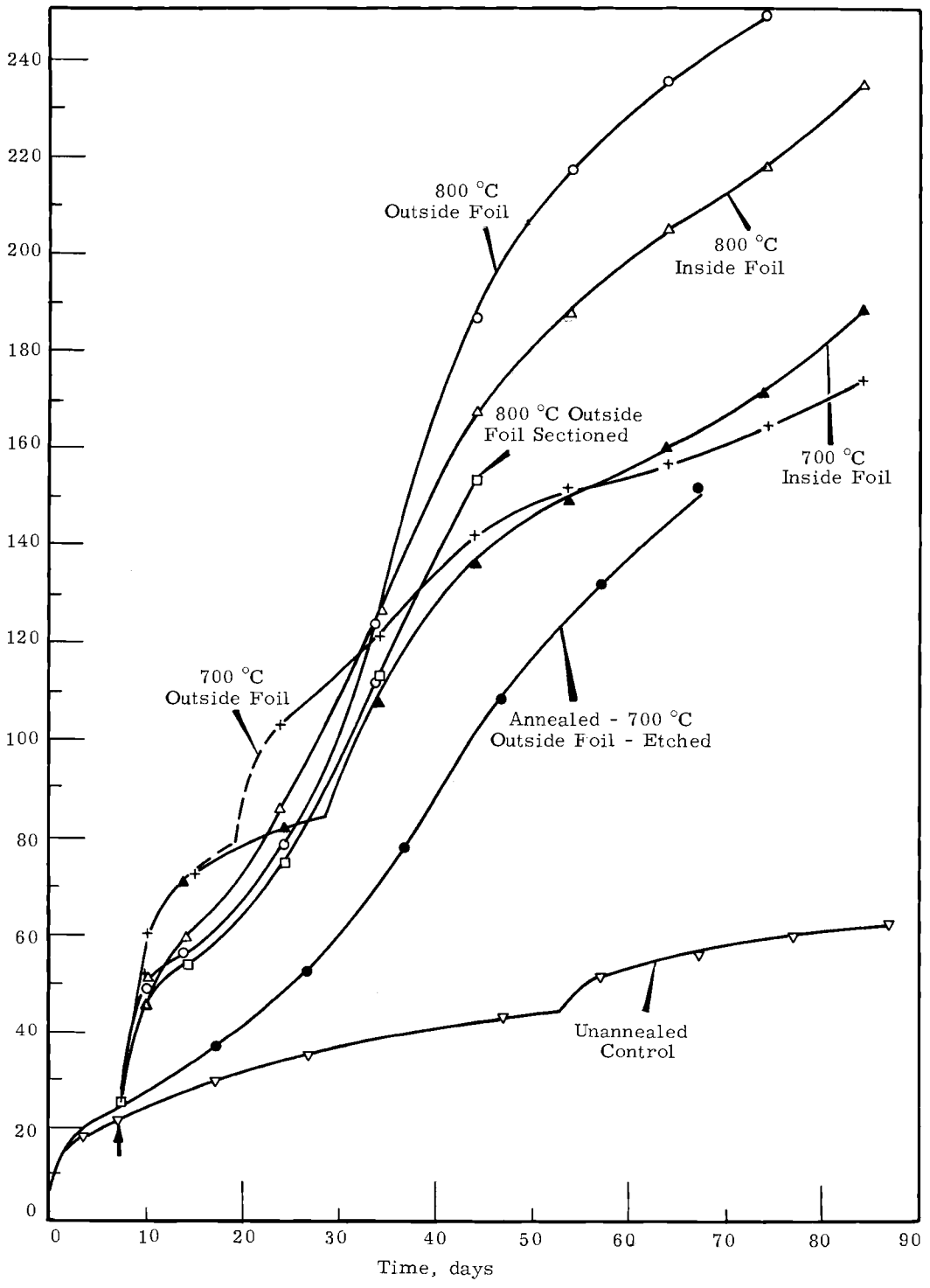

FIGURE 5.1

Oxidation of Zircaloy-2 in Steam at 400 °C,
Following Vacuum Annealing of 20 mg/dm^2 Oxides

(Figure 5.2). Pemsler[1] suggested that the oxygen-rich layer may be unable to support thick oxide films, resulting in cracking of both oxide and metal. Additional samples will be sectioned to see if the cracks correlate

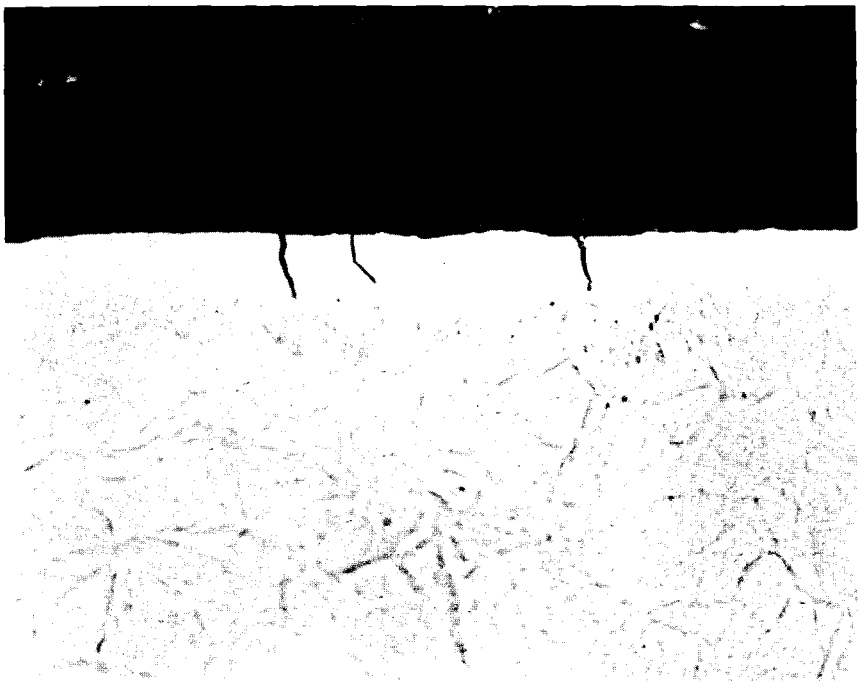

500X

FIGURE 5.2

Cracks in Oxygen-Rich Metal Zone
on Vacuum Annealed Zircaloy-2

Coupon History

Oxidized - 20 mg/dm^2
Vacuum Annealed - 70 min, 800 °C
Autoclaved - 44 days (total) 400 °C, Steam
Sectioned - Polished, Cathodically Etched

reproducibly with accelerated oxidation. Further work on the effect of etching will be conducted to see how both the first and second accelerated attacks are affected by various degrees of metal removal.

(1) J. P. Pemsler. "Studies on the Oxygen Gradients in Corroding Zirconium Alloys," J. Nuclear Materials, vol. 7, pp. 16-24. 1962.

Neg. 465648B

MATERIALS ENGINEERING UNIT

PRTR PRESSURE TUBES - M. C. Fraser

The PRTR pressure tubes were fabricated from Zircaloy-2 ingots by a forging-hot-extrusion-tube reduction process. These tubes have a unique shape, one end is flanged and the other tapers to a reduced section. They also have a unique microstructure; there is an annealed region between the taper and the flange, the rest is cold worked. The ability of these tubes to sustain the imposed PRTR system loads with ever increasing neutron exposure has been a subject of study and testing since reactor startup. The following paragraphs describe the study and testing done during the last quarter year.

Properties of Irradiated PRTR Pressure Tubes

In preparation for stress rupture testing of irradiated tube specimens, an experiment is being performed to determine if a temperature of 550 °F will cause significant annealing of irradiation damage. The most recently obtained information indicates that 2000 hr at 550 °F will not significantly change the strength or ductility of Zircaloy-2 tube specimens whose fast neutron exposure is 5×10^{20} nvt ($E > 1$ MeV).

A tube was discharged from the reactor. One piece of this tube was burst tested at room temperature. The pressure in this specimen was raised to 13,250 psi before localized necking and then bursting occurred. The other piece was crack-propagation tested at room temperature. A 1 in. long crack propagated the length of the specimen when the internal pressure reached 5980 psi.

These failure pressures are equal to or greater than failure pressures of comparable specimens having lower neutron exposure. Swelling of the burst test specimen and shear fracture of the crack propagation specimen occurred to indicate ductility was present. The test indications are that the tubes are still suitable for use in the reactor environment.

Properties of Unirradiated PRTR Pressure Tubes

Measurement of the elastic constants of tube specimens will reveal the degree of anisotropy of the circular cylindrical bodies. Evidence that they are anisotropic has been obtained by measurement of elastic hoop and axial strain on the outside surface during the imposition of various combinations of internal pressure and axial load. This evidence is presented in Figure 6.1. The ratio of axial to hoop strain is shown by solid lines to be a function of a quantity R. The equation expressing this function is

$$\frac{\varepsilon_z}{\varepsilon_\theta} = \frac{R - \nu}{1 - R\nu} \tag{1}$$

where ν is Poisson's ratio and R is called load ratio. Equation (1) comes from analysis of the expansion of an isotropic cylindrical tube under the influence of an internal pressure and an axial load. The broken line in Figure 6.1 shows the variation of the ratio of measured strain with load ratio for an unirradiated PRTR Zircaloy-2 tube specimen. It is apparent that the specimen's elastic response to increasing load ratio is significantly different from the predicted isotropic case.

The term "load ratio" is defined by

$$R = \frac{Pa^2\pi + F}{2\,Pa^2\pi} \tag{2}$$

where P is internal pressure, a is tube inside radius, and F is an axial force. For an isotropic thin wall tube, Equation (2) is equivalent to the ratio of average stress; but for an anisotropic case, it is not equivalent to the ratio of average stress. This is why Equation (2) is defined as load ratio.

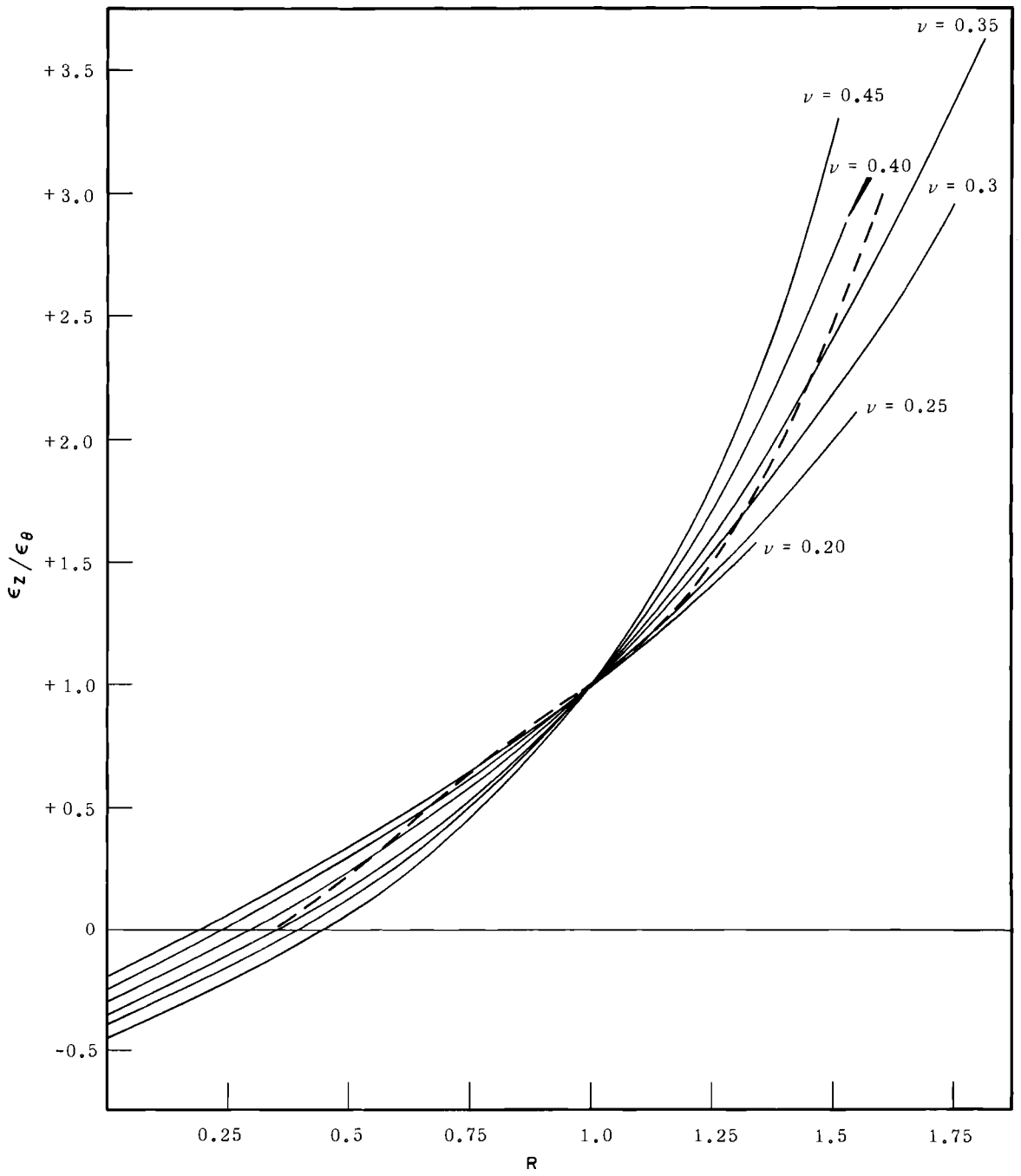

FIGURE 6.1

An Unirradiated PRTR Zircaloy-2 Tube Specumen (broken line) is Anisotropic by Comparison with a Theoretical Isotropic Tube (solid lines)

GAS LOOP DEVELOPMENT

The model gas loop is a 2000 °F, 500 lb/hr flow, helium recirculating loop that is approximately a one-tenth model of the ATR Helium Loop that is designed for installation in the Advanced Test Reactor (ATR) at Idaho Falls. The ATR loop will be used for irradiation damage studies on refractory metals and with some modifications could be used to irradiate fuel samples. One important function of the model loop is to support the design of the ATR loop. This function is nearly complete except for the gas heater which is in the design phase. The heater design represents a significant departure from the commercial practice, therefore, a similar type of heater is being built for the model loop.

There are two gas cleanup systems associated with the model loop. One is a high pressure single pass system that takes relatively impure helium and after cleanup feeds the pure gas into storage bottles at 2000 psi or into the loop at pressures up to 300 psi. A goal of less than 1 ppm total impurities for the discharge from this system is routinely achieved when the input gas has a water content of less than 15 ppm. The second system by-passes a portion of the model loop recirculating helium, purifies it and then returns it to the loop. A similar purity goal of less than 1 ppm total impurities has been difficult to achieve because of leaks in the numerous mechanical joints in the model loop.

Other work in support of the ATR this quarter has involved bench tests on a mock-up of a seal between the in-core 347 SS pressure tube of the ATR helium loop and the Columbium sleeve liner for this tube. Also, a mechanical tubing fitting was tested for application on the ATR loop where it is impractical to use a welded joint, and some pressure drop data was obtained from the model loop regenerative heat exchanger.

Model Loop Helium Cleanup

Improvements in the bypass cleanup system have made it possible to clean the gas to less than 1 ppm total impurities at low temperatures. Test runs will be made to determine if this low impurity level can be maintained at higher temperatures.

Columbium Sleeve Leak Test - L. J. Defferding

The specimen assembly and the 2000 °F helium in the test section of the ATR Gas Loop will be separated from the in-reactor pressure tube by a columbium sleeve heat shield. The labyrinth seal at the top of the sleeve must reduce helium flow through the annulus between the pressure tube and the sleeve to 25 lb/hr or less at a sleeve temperature of 2000 °F and a pressure drop of 30 psi in order to prevent excessive heat loss to the water jacket surrounding the pressure tube. A test apparatus was constructed to check the leakage past the labyrinth seal. A sleeve with a diametral clearance of 0.010 in. produced a leakage of 8.9 lb/hr at 1000 °F with a pressure drop of 35 psi. A second sleeve with a diametral clearance of 0.023 in. produced a leakage of 30.4 lb/hr at 1000 °F and a pressure drop of 20 psi. Heater failures in the test section have prevented the completion of testing to the desired sleeve temperature of 2000 °F. When modifications to the heater are completed further test runs will be made.

Mechanical Tubing Connector Leak Test - L. J. Defferding

A mechanical tubing connector was tested for helium service. The connector was temperature cycled between -190 and 160 °C. One connector was disassembled and reassembled 15 times. No leaks occurred on any of the tests with the helium pressure at 2100 psig.

Model Loop Regenerative Heat Exchanger - L. J. Defferding

Instrumentation was installed on the model gas loop to measure the pressure drop in both the shell and tube sides of the regenerative heat exchanger. The loop was operated at several flow rates from 100 to 375 lb/hr with the heater outlet temperature varying from 210 to 2100 °F. The maximum pressure drop across the shell was 16.5 in. of water while the drop across the tube was 9.5 in. of water. The gas bearing compressor has operated a total of 560 hr with 126 starts.

Model Gas Loop Heater and Piping Modifications - R. J. Evans

Initial assembly has begun on a model gas loop heater designed to incorporate and investigate essential details of a compact two-stage, concentric heater being designed for the ATR Gas Loop. Major design features of this heater are described in previous quarterly reports.[1, 2, 3]

Metallic foil insulation sections for the heater and piping internal insulation are 90% complete. Unique sections of insulation designed to fit the inside of the heater and allow no direct radiant path to the outer shell were made by rolling sheets of foil into cylinders (30 layers per in.), filling the cylinders with water, freezing with liquid nitrogen and machining. The insulation was then thawed and baked in a furnace to drive off remaining moisture. Final insulation work will be completed shortly after model loop modification pipe fittings are delivered. Insulation must be sized to each fitting because of the large dimensional tolerance in commercial pipe fittings.

The pipe has arrived and water jackets are being placed on sections that will be used for modification of the loop.

Heating element tubes for each stage of the heater will be connected to its neighbor and to power supply electrodes to form a series electrical circuit. Since it is desirable to minimize connector heat losses, good contact between the tube and the connector must be made. Joining of the molybdenum heating tubes to their molybdenum connectors has been investigated.[3] Expansion of the tubes into the connectors by rolling failed. The

---

1. Quarterly Progress Report, Metallurgy Research Section, October, November, December, 1964, edited by J. J. Cadwell, HW-84573. General Electric Company, Richland, Washington. January 15, 1965.
2. Quarterly Progress Report, Metallurgy Research Section, January, February, March, 1965, edited by J. J. Cadwell, BNWL-79. April 15, 1964.
3. Quarterly Progress Report, Metallurgy Research Section, April, May, June, 1965, edited by J. J. Cadwell, BNWL-120. July 15, 1965.

tubes cracked in tests from room temperature to 300 °F. Shrink fitting was also not successful. Press fitting, using a straight hole-straight tube with a 0.2 mil interference and a tapered hole-tapered tube were satisfactory. Tests to determine if these connections will hold at operating temperatures are now being conducted.

All nichrome and molybdenum heating element tubes were non-destructively tested for flaws and wall thickness variations. Due to trouble with the test equipment 4 of the 15 nichrome tubes could not be measured; the others were satisfactory. Four of the 9 molybdenum tubes received were so badly striated on the inside that ultrasonic thickness measurements could not be made. Two of the remaining five molybdenum tubes had thin wall sections and are unacceptable for use in the heater.

Flexible connectors, made with stacked nickel sheets, to take up thermal expansion between internal and external electrodes were not flexible enough to be used. The 25 mil sheets are being replaced by nickel braid of equivalent current carrying cross-section. Some redesign of the connectors may be necessary.

Electrical work on items that do not interfere with present operation of the loop has been completed.

N-REACTOR - R. C. Aungst

Fracture Studies

Tests to determine the resistance of pressure tubing to brittle fracture have been developed in this laboratory and discussed in an earlier report.[1] These are tests on complete sections of tubing pressurized to failure in the presence of a flaw. Within their scope these tests provide reassuring evidence to the reactor operators that brittle fracture is not likely to be a limiting factor in safe operation. However, rather than using specifically aimed engineering tests of this type, it has been more common in the literature for authors to consider fracture behavior in terms of nil ductility transition (NDT) temperatures and of the fracture analysis diagram as developed by Pellini and Puzak.[2] In response to this trend we have developed a drop-weight test to determine an NDT temperature on specimens cut from the wall of N-Reactor pressure tubing and have constructed a modified fracture analysis diagram from the results of fracture tests on slotted tube specimens over a range of temperature.

The principle of the drop-weight test involves the starting of a crack in the tension side of a specimen when it is bent through a limited angle by the impact of a falling weight. The test determines the temperature at which the crack propagates entirely across the test specimen. The starting of the crack is assured by the presence of a small strip of hydrogen-embrittled Zircaloy, resistance welded to the tension side of the specimen. The specimen as finally evolved for this test is a quadrant cut from a 1 in. ring removed from the tube. The falling weight strikes the convex surface of the piece and straightens it out by an amount limited by a stop placed beneath the arch of the specimen.

---

1. R. C. Aungst and L. J. Defferding. Crack Propagation Tests on Normal and Hydrided Zircaloy-2 Reactor Pressure Tubing. HW-80567. General Electric Company, Richland, Washington. August, 1964.
2. W. S. Pellini and P. P. Puzak. Fracture Analysis Diagram Procedures for the Fracture-Safe Engineering Design of Steel Structures, NRL-5920. Naval Research Laboratory. March 15, 1963. Also Welding Research Council Bulletin Series No. 88. May, 1963.

Specimens cut from N-Reactor tubing representing two different fabrication processes and several levels of hydride concentration have been subjected to the drop-weight test. The results as plotted in Figure 6.2 show the relationship between NDT and hydrogen content. In general the transition temperature is shown to rise with increasing hydrogen content. However, at least two interpretations are apparent from a detailed analysis of the distribution of the points. If the points for the drawn tubing are connected and those for the tube reduced material are independently connected, the result is two curves, one considerably below the other. This analysis would indicate a marked difference in the two types of material. The reason for such a marked difference is not readily apparent. Pole figures[1] show virtually no difference in texture, and metallography shows similar grain size and configuration in both types of tubing. A second interpretation of the data is represented by the dashed line which attempts to account for all the points. This would not indicate a difference between the two types of material, but instead an extreme sensitivity to hydrogen in concentrations below 25 ppm. Additional tests at extremely low and at intermediate levels of hydrogen content are planned in an attempt to clarify these relationships.

Farrow and Watkins at the Culcheth Laboratories of UKAEA have conducted similar tests[2] on 20% cold worked Zircaloy-2 tubing. They report an NDT of 110 °C at a hydrogen content of 200 ppm. This value when plotted (Figure 6.2) with our data is not inconsistent with either interpretation discussed above.

---

1. R. C. Aungst and L. J. Defferding. Crack Propagation Tests on Normal and Hydrided Zircaloy-2 Reactor Pressure Tubing, HW-80567. General Electric Company, Richland, Washington. August, 1964.
2. M. Farrow and B. Watkins. "The Effect of Hydrogen on the Embrittlement of Zirconium-Base Pressure Tubes," J. Nuclear Materials, vol. 15, no. 3, pp. 208-219. 1965.

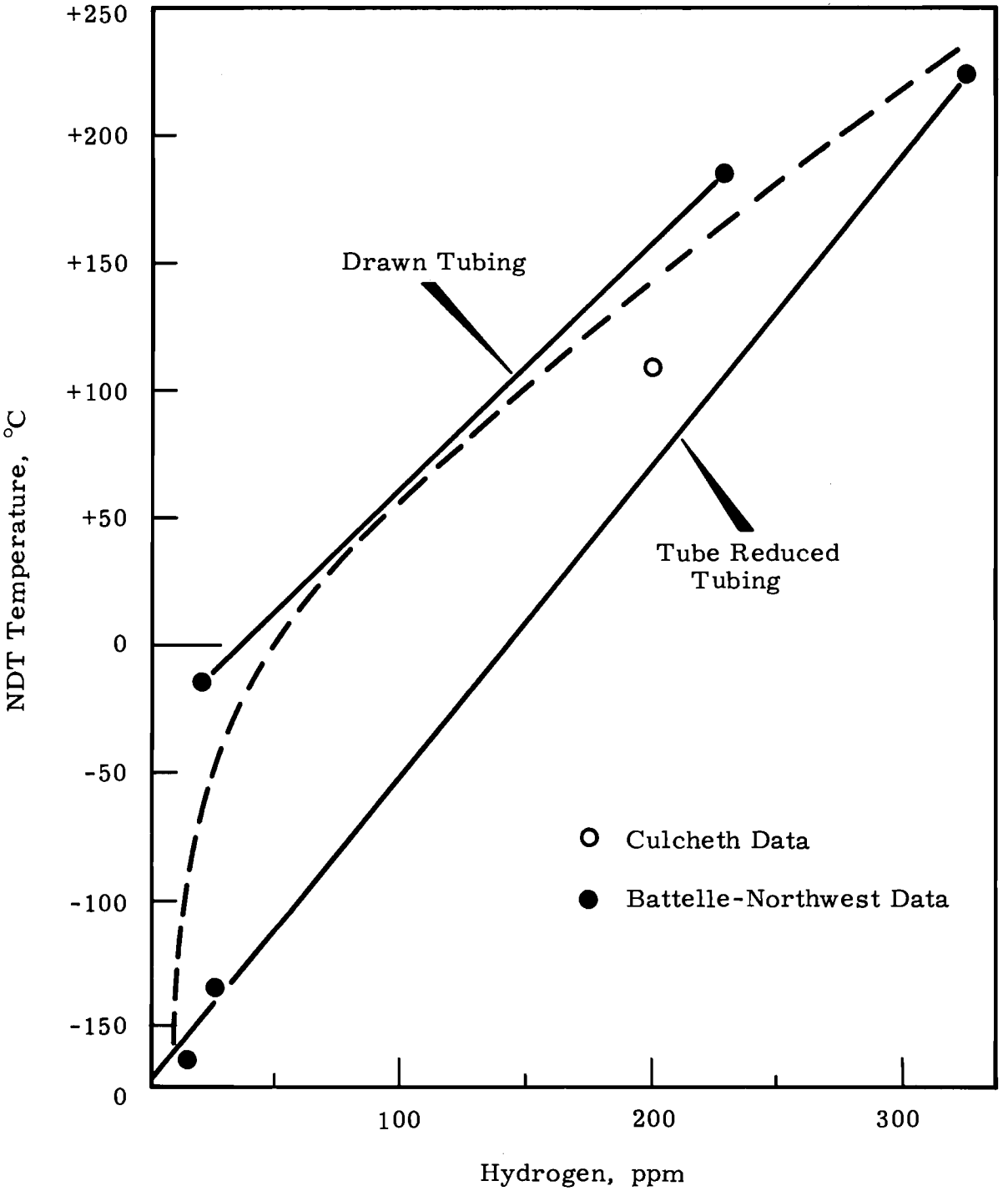

FIGURE 6.2

Drop-Weight Specimens from 20-30% Cold Worked Zircaloy-2 Tubing

Fracture Analysis Diagram

The fracture analysis diagram as developed for steel at the Naval Research Laboratory is shown in Figure 6.3. It shows a sharp rise in the crack initiation curves above the NDT. These rising curves are bounded on the right by a crack arrest temperature (CAT) curve that defines a temperature limit above which propagation cannot occur. An attempt to fit the results of crack propagation tests on slotted tube specimens to this type of curve produced the diagram in Figure 6.4. Note that all the tests for a given flaw size show failure at the same percentage of yield throughout the temperature range. This is typical of behavior below the NDT in the standard diagram for steel and shows none of the rising trend that would be expected above the NDT. As temperatures approach the upper limit of the range tested, a point is reached where the tube no longer fails by full length brittle fracture. Instead the test is terminated by relief of pressure through a slight extension of the crack by ductile tearing. This transition defines a CAT curve.

This modified fracture analysis diagram thus differs in several respects from the standard diagram for steel. The flatness of the curves throughout the entire temperature range tends to minimize the significance of the NDT as a measure of performance of a Zircaloy-2 tube tested under biaxial conditions. However, the crack arrest temperature appears to be a useful parameter in predicting the type of failure to expect under given conditions. The apparent anomalies in this diagram may reflect differences in geometry and methods of testing as much as they reflect material differences between Zircaloy and steel. In developing the diagram for tubing, the stress system was complicated by biaxiality and the presence of bending stresses from the opening of the slot-type defect.

The most useful part of this modified fracture analysis diagram is the CAT curve. Future work will deal with establishing this curve for materials with different fabrication histories and with various hydride contents and modes of hydride dispersion. If a reasonably rigorous relationship

can be demonstrated between the drop-weight NDT and the CAT, the drop-weight test with its greater economy of material may become a valuable tool for investigating the effects of irradiation and other variables.

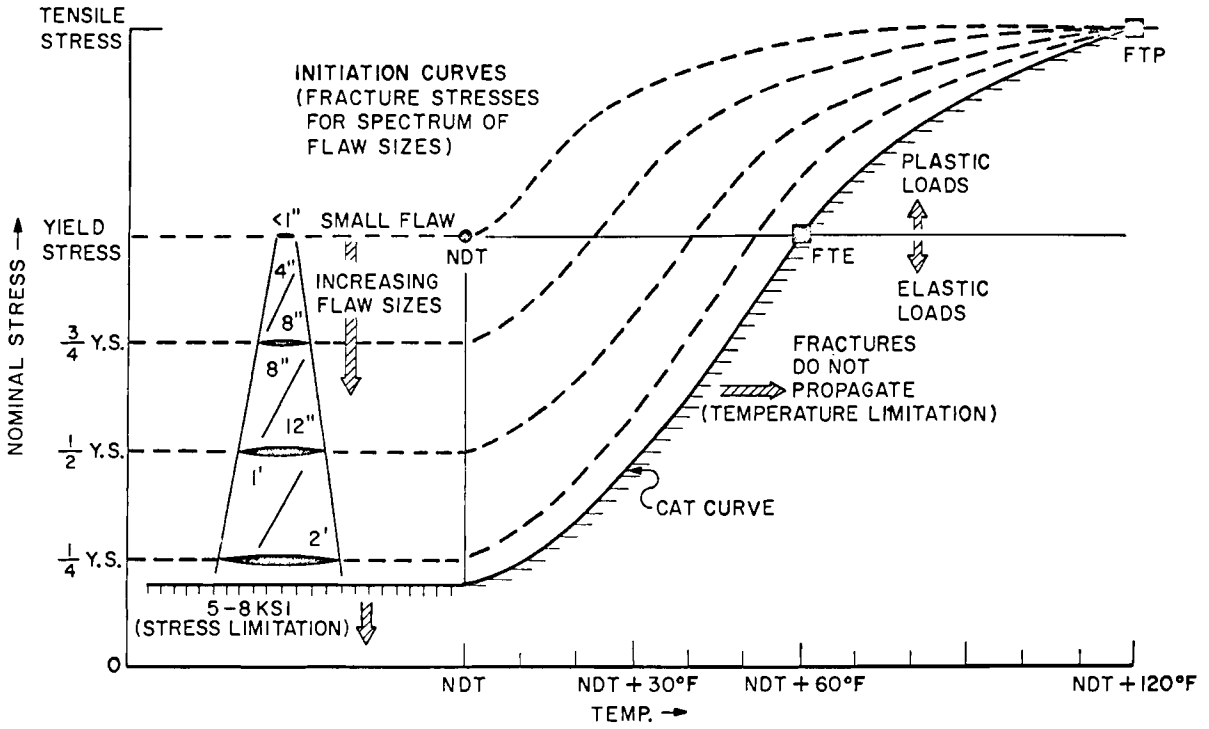

FIGURE 6.3

Generalized Fracture Analysis Diagram
(as referenced by the NDT temperature)

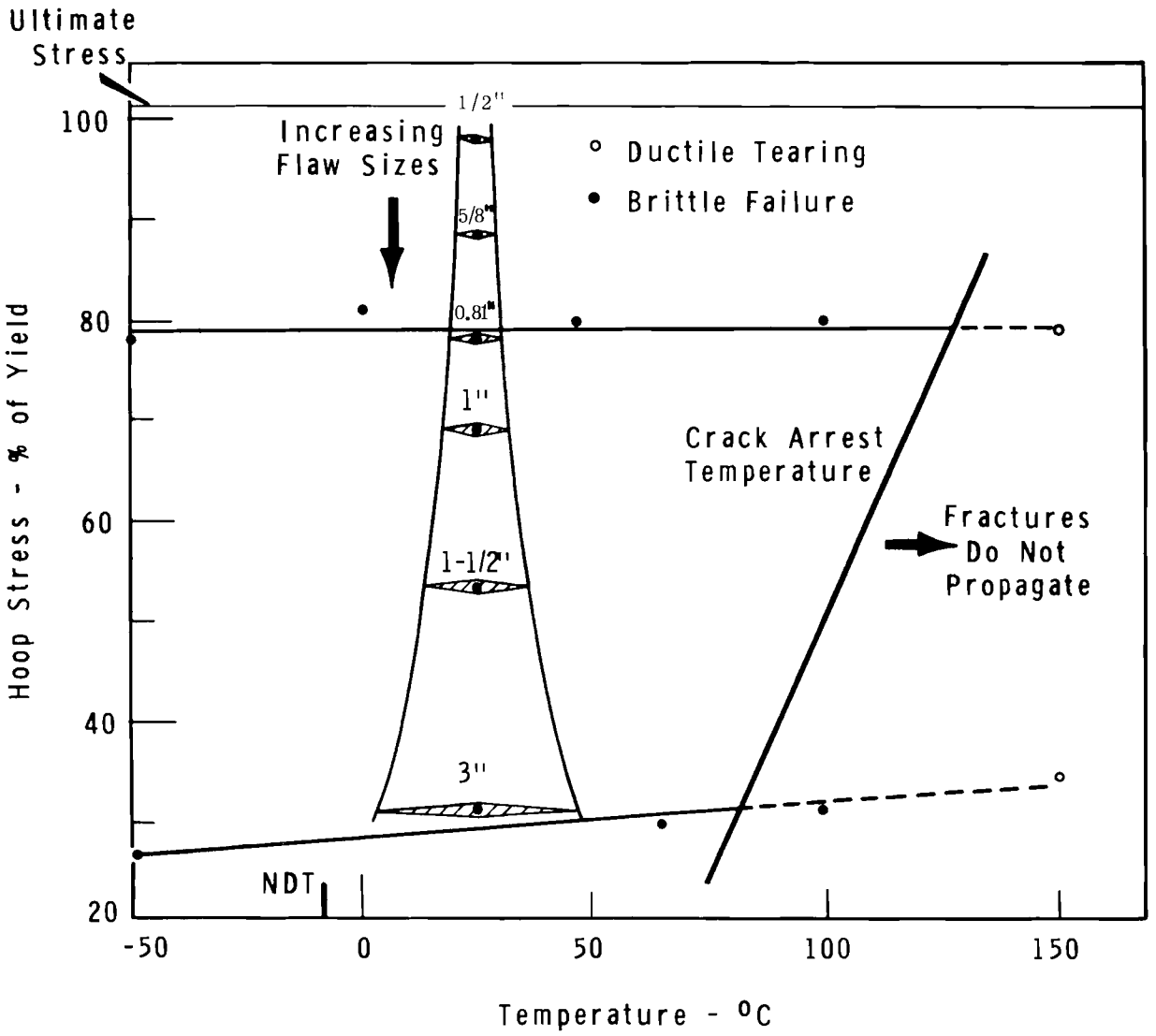

FIGURE 6.4

Modified Fracture Analysis Diagram
for Pressurized Zircaloy-2 Tubing

USA-AECL COOPERATIVE PROGRAM - P. J. Pankaskie

Zr-Nb Pressure Tubing

Tubular specimens 2 in. ID x 0.180 in. wall, were tested under biaxial stress conditions to determine the crack propagation characteristics of this material when hydrided to concentration levels of about 250-300 ppm (corresponds to solubility limit at about 400 °C). In these tests the ratio of hoop to axial stress was two to one. Prior to hydriding a slot, 1/16 in. wide with a depth equal to 80% of the wall thickness, was milled in the outside surface at about the mid-length of the test specimen. Slot lengths varied from 1/2 to 2 1/2 in. After hydriding at 400 °C, about 0.010 in. of the outside surface was removed to assure a uniformly hydrided test specimen. The results of the three tests now completed are shown in the following table.

CRACK PROPAGATION DATA FOR HYDRIDED ZR-2.5 wt% Nb ALLOY

Specimen Identification	Specimen Condition % Cold-Worked	Test Temperature, °C	Slot Length, in.	Hoop Stress at Failure, psi	Crack Length After Failure
30-7	30	25	1 1/2	31,400	Brittle behavior crack propagated full length of test piece
30-10	30	25	2 1/2	28,000	Brittle behavior crack propagated full length of test piece
60-9	60	25	2 1/2	8,300	Brittle behavior crack propagated full length of test piece

The strength behavior of this alloy in the hydrided condition appears to be somewhat erratic. For the 1 1/2 in. long slot, the hoop stress at failure is reduced moderately while for the 2 1/2 in. long slot the strength is increased slightly as compared with nonhydrided test specimens. For the 60% cold worked condition, the strength of a hydrided test specimen with a 2 1/2 in. long slot is substantially lower than for nonhydrided material. More testing is needed to define the crack propagation characteristics of this alloy in the hydrided condition.

A series of tensile tests were made on test specimens machined from Zr-2.5 wt% Nb alloy tubing. In all cases, the test specimen axis was parallel to the tube axis. Data were obtained for tests at temperatures of

23, 300, and 400 °C and strain rates of 0.002, 0.050, and 0.500 in./in./min. These data are shown in Figures 6.5, 6.6, and 6.7. These data show that there is little or no effect of strain rate on either strength or ductility at 23 and 300 °C. At 400 °C the yield and ultimate strength increases and the ductility decreases as the strain rate increased. These differences in strength and ductility may be due in part to recovery effects since the slower strain rates provide appreciably more time for recovery to take place.

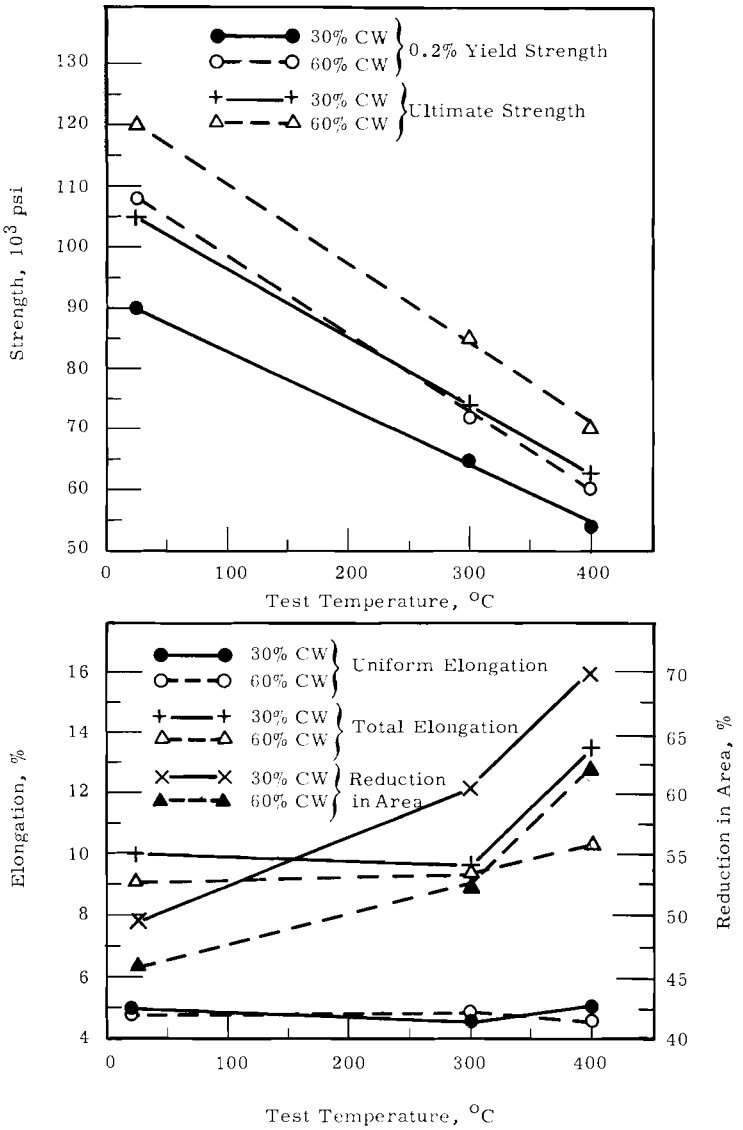

FIGURE 6.5

Tensile Properties of Zr-2 1/2 wt% Nb Alloy Versus Temperature, and at a Strain Rate of 0.002 in./in./min

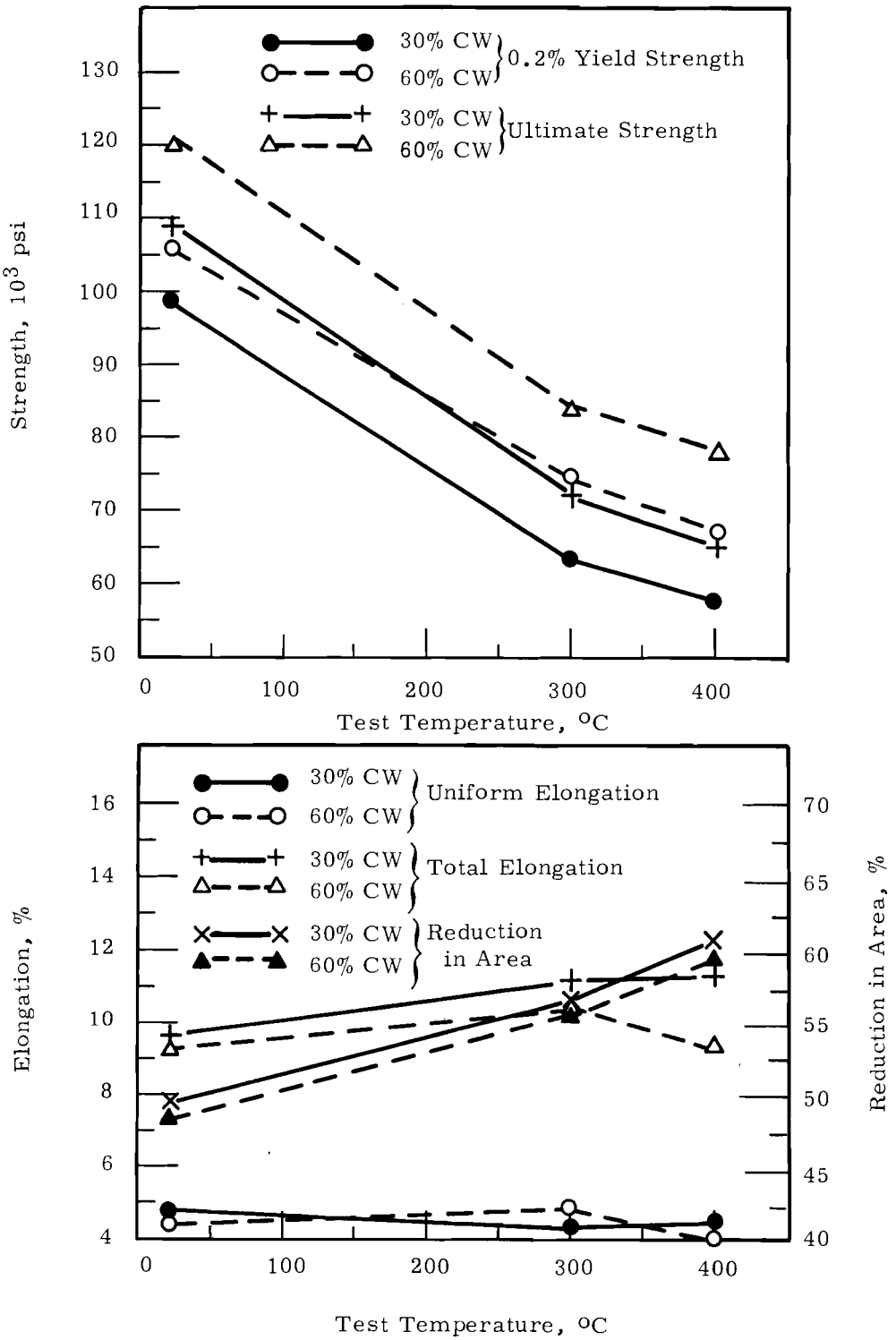

FIGURE 6.6

Tensile Properties of Zr-2 1/2 wt% Nb Alloy
vs Temperature and at a Strain Rate of 0.050 in./in./min

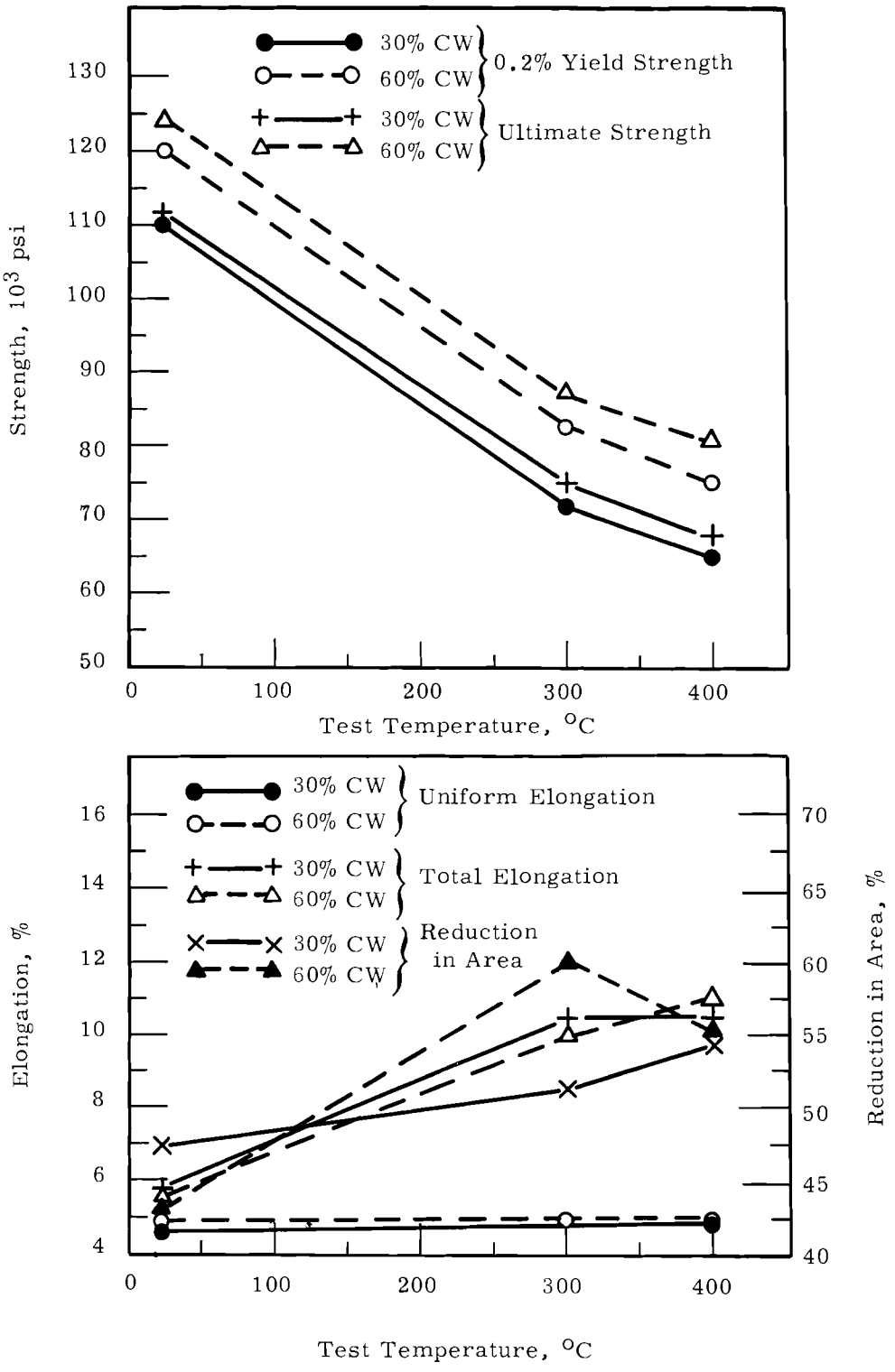

FIGURE 6.7

Tensile Properties of Zr-2 1/2 wt% Nb Alloy
vs Temperature and at a Strain Rate of 0.500 in./in./min

ONSITE DISTRIBUTION

Copy Number	Pacific Northwest Laboratory
1	F. W. Albaugh
2	T. W. Ambrose
3	J. A. Ayres
4	J. M. Batch
5	A. L. Bement
6	C. A. Bennett
7-8	T. K. Bierlein
9	S. H. Bush
10	J. J. Cadwell
11	T. T. Claudson
12	L. L. Crawford
13	G. M. Dalen
14	D. R. de Halas
15	R. F. Dickerson
16	R. L. Dillon
17	K. Drumheller
18	E. A. Eschbach
19	W. E. Foust
20	J. C. Fox
21	W. L. Hampson
22	L. A. Hartcorn
23	H. Harty
24	R. S. Kemper
25	H. A. Kornberg
26	G. A. Last
27	J. E. Minor
28	R. D. Nelson
29	R. E. Nightingale
30	D. P. O'Keefe
31	H. M. Parker
32	R. S. Paul
33	W. E. Roake
34	R. E. Skavdahl
35	F. A. Smidt
36	D. R. Stenquist
37	C. R. Tipton
38	M. T. Walling
39	R. D. Widrig
40-41	R. G. Wheeler
42	F. W. Woodfield
43	O. J. Wick
44	H. H. Yoshikawa
45-49	Technical Information Files
50-51	Technical Publications - 700 Area

ONSITE DISTRIBUTION

Copy Number

General Electric Company, Richland

52	D. H. Curtiss
53	R. L. Dickeman
54	T. W. Evans
55	J. M. Fox, Jr.
56	S. M. Graves
57	M. C. Leverett
58	C. G. Lewis
59	M. Lewis
60	L. M. Loeb
61	J. W. Nickolaus
62	J. W. Riches
63	GETA File Copy

Richland Operations Office

64-65	R. K. Sharp
66	Technical Information Library

OFFSITE DISTRIBUTION

No. of Copies

2	Atomic Energy Commission, Washington Division of Research Attn: Don K. Stevens Dorothy Smith
2	Atomic Energy Commission, Washington Division of Reactor Development Attn: J. M. Simmons W. R. Voigt
1	Battelle Memorial Institute Radiation Effects Information Center Attn: W. H. Veazie
3	Center for Nuclear Studies at Saclay P.O. Box 2 Gif-sur-Yvette (Seine-et-Oise) France Attn: Thomas de Montpreville
1	Dow Chemical Company, Rocky Flats Attn: Robert D. Forest

OFFSITE DISTRIBUTION (Special)(contd)

No. of Copies	
1	Combustion Engineering, Inc. P.O. Box 500 Windsor, Connecticut 06095 Attn: W. P. Chernock
1	European Atomic Energy Community (EURATOM) 51-53 rue Belliard Brussels, Belgium Attn: Pierre Kruys
1	General Electric Company Advanced Products Operation 175 Curtner Avenue San Jose, California 95103 Attn: F. Comprelli
1	H. J. Pessl Route 1, Box 892 Hood River, Oregon 97031
1	Structural Materials Laboratory Aktiedolaget Atomenergi Studsvik, Sweden Attn: Mikael Grounes, Head
1	University of California, Berkeley Attn: J. F. Dorn
1	University of Florida Metallurgical Research Laboratory College of Engineering Attn: R. T. de Hoff
1	University of Michigan Attn: M. J. Sinnott